Interval Velocity Classification Technique in Downhole Seismic Testing

by Erick Baziw and Gerald Verbeek

ABSTRACT

Downhole Seismic Testing (DST) is an important geotechnical testing technique for site characterization that provides low strain in-situ interval compression and shear wave velocity estimates, which are fundamental design parameters for static and dynamic soil analysis. A challenging problem in DST is to obtain an accurate assessment of the quality of the calculated interval velocities. This paper describes in detail a newly developed Interval Velocity Classification (IVC) technique for DST interval velocity estimations. This technique uses three independent seismic time series characteristics: 1) The cross-correlation coefficient calculations of the full waveforms between successive depths of data acquisition. 2) Linearity estimates from the polarization analysis of triaxial or biaxial sensor packages. 3) A new seismic time series characteristic parameter that quantifies the deviation of the source wave frequency spectrum from a desirable bell-shaped curve. The paper also includes examples where this technique was applied on real data sets to demonstrate how results of the IVC technique can direct the investigator to possible approaches for improving the signal to noise ratios of the acquired seismic traces.

INTRODUCTION

A fundamental goal of geotechnical *in-situ* testing is the accurate estimation of the shear and compression wave velocities (V_P and V_S, respectively) in the ground. These parameters form the core of mathematical theorems to describe the elasticity/plasticity of soils and they are used to predict the soil response (settlement, liquefaction or failure) to imposed loads (whether from foundations, heavy equipment, earthquakes or explosions) (Finn 1984; Andrus et al. 1999, 2000; Ishihara 1982). Accuracy in the estimation of shear and compression wave velocities is of paramount importance because these values are squared during the calculation of various geotechnical parameters such as the Shear Modulus (G), Poisson's Ratio (μ) and Young's modulus (E).

Downhole Seismic Testing (DST) such as Seismic Cone Penetration Testing (SCPT) (Campanella *et al.*, 1986; Baziw, 1993; ASTM, 2013) is a common geotechnical technique for measuring *in-situ* V_S and V_P velocities. The main goal in DST is to obtain arrival times as the source wave travels through the soil profile of interest, and from these arrival times the V_S and V_P velocities are then calculated. Figure 1 shows a schematic of the typical DST configuration.

Obviously it is highly desired to assign an accuracy or confidence level to the estimated interval velocities. Typically, investigators have utilized the Cross-Correlation Coefficient (CCC), which gives an indication of the similarity between traces used in obtaining relative arrival times (Baziw, 1993), but this parameter has been proven to be an unreliable indicator due to the fact that measurement noise (random and systematic) can also be correlated and result in high CCC values. In order to overcome these limitations a new and significantly more comprehensive approach to DST interval velocity assessment and classification was developed, which applies an interval velocity classification similar to the methodology Ge (Ge and Mottahed, 1993 and 1994; Ge, 2003) developed for microseismic source location estimation. This methodology takes various information sets from the acquired microseismic data for each event and subsequently fuses these information sets together based upon analytic, derived and evolving empirical relationships. The outcome is that a microseismic source location estimate "Rank" is obtained, varying from A (very good), B (good), C (acceptable), D (questionable) to F (unacceptable).

The work in this paper outlines the efforts to develop a similar ranking or classification technique for DST interval velocity estimation. Similar to Ge, the objective is to incorporate other independent parameters with the CCC (since only independent parameters can add additional information) into the quality assessment so that a more robust classification technique is established. This paper outlines a new DST Interval Velocity Classification (IVC) where three independent parameters are fused together to generate an assessment or classification of the estimated interval velocities. The three seismic time series characteristics are the cross-correlation coefficient calculations of the full waveforms between successive depths of data acquisition, linearity estimates from the polarization analysis of triaxial or biaxial sensor

packages, and a new seismic time series characteristic parameter that quantifies the deviation of the source wave frequency spectrum from a desirable bell-shaped curve.

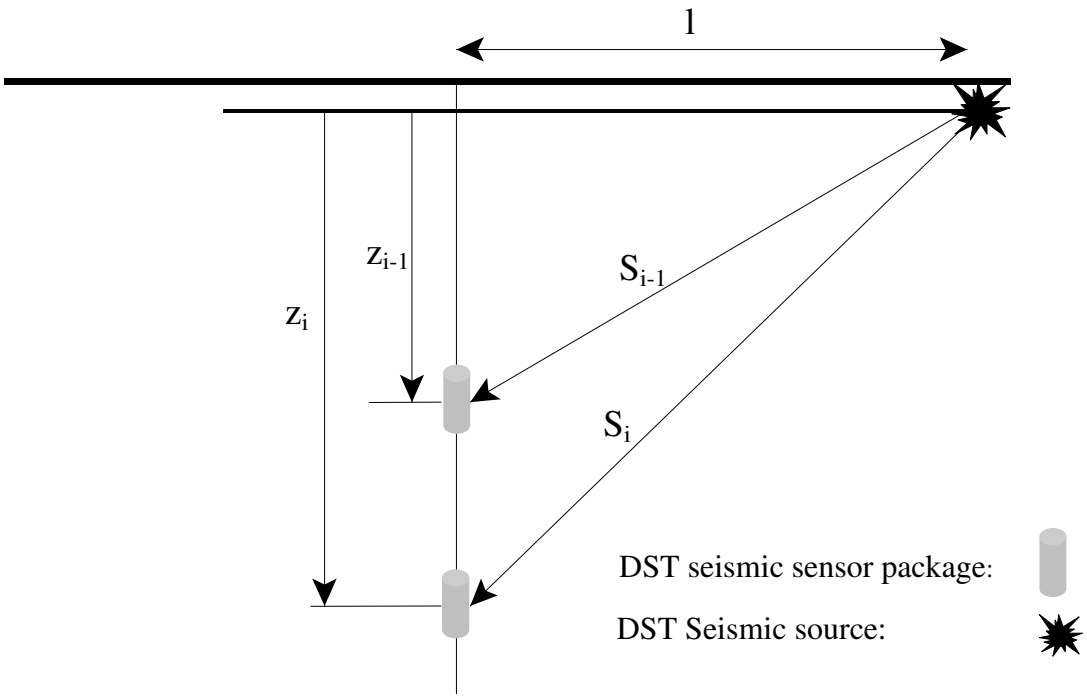

Figure 1: Schematic of the typical DST configuration.

THE IVC TECHNIQUE

Information Set 1: Cross- Correlation Coefficient

The cross-correlation between two time or distance offset seismograms is given as[1] (Gelb 1974)

$$\varphi_{xy}(\tau) = \sum_k X_k \, Y_{k+\tau} \tag{1}$$

where $\varphi_{xy}(\tau)$ is the cross-correlation function, Y_k the sampled data at distance 1 and at sample time k, X_k the sampled data at distance 2 at sample time k, and τ the time shift between the two sets of recorded waves (note: distance 2 > distance 1). The value of the time shift at the maximum cross-correlation value is assumed to be the relative travel time difference, Δt, for the source wave to travel the distance increment. This technique has several

[1] Typically the mean of the seismic signals is removed prior to applying the cross-correlation function. The cross-correlation of zero mean signals is identical to the covariance.

advantages (Baziw 1993, 2002) over selecting time markers within the seismogram, among others the human bias associated with visually selecting a reference point or time marker is minimized.

Normalizing the cross-correlation of the zero mean seismic signals by their standard deviations gives the cross-correlation coefficient:

$$\rho_{xy}(\tau) = \sum_k X_k Y_{k+\tau} \Big/ \sqrt{\sum_k X_k^2} \sqrt{\sum_k Y_K^2} \tag{2}$$

As mentioned before, the CCC between the two DST waves is typically used to assess the quality of the interval velocity estimate as this parameter gives an indication of the similarity between the two waves being correlated. Unfortunately, on its own the correlation coefficient has proven to be an unreliable indicator, since it is highly dependent on the digital filter applied to the raw seismic signals, the cross-correlation time window as well as the presence of correlated measurement noise. For example, Fig. 2 illustrates low SNRs data acquired at depths 10.6 m and 11.6 m that was filtered with a 300 Hz low pass filter. Applying (1) on these data for the time window of 47 ms to 130 ms (as denoted by the thick bold and dashed vertical lines) results in the cross-correlation function illustrated in Fig. 3 with a corresponding CCC of 0.7387. However, a bandpass digital frequency filter of 30 Hz to 100 Hz on the same SCPT data results in the filtered data shown in Fig. 4, and applying (1) on these data for the identical time window generates the cross-correlation function illustrated in Fig. 5 with a corresponding CCC of 0.9136. The percent difference between the CCC values 0.9136 and 0.7387 is 21%. For this reason the authors have recommended that minimal filtration is applied when calculating the CCC, but even then this parameter is not necessarily reliable. This is due to the fact that additive measurement noise can be correlated, is illustrated with a real data set example given in Section 2.3.3.

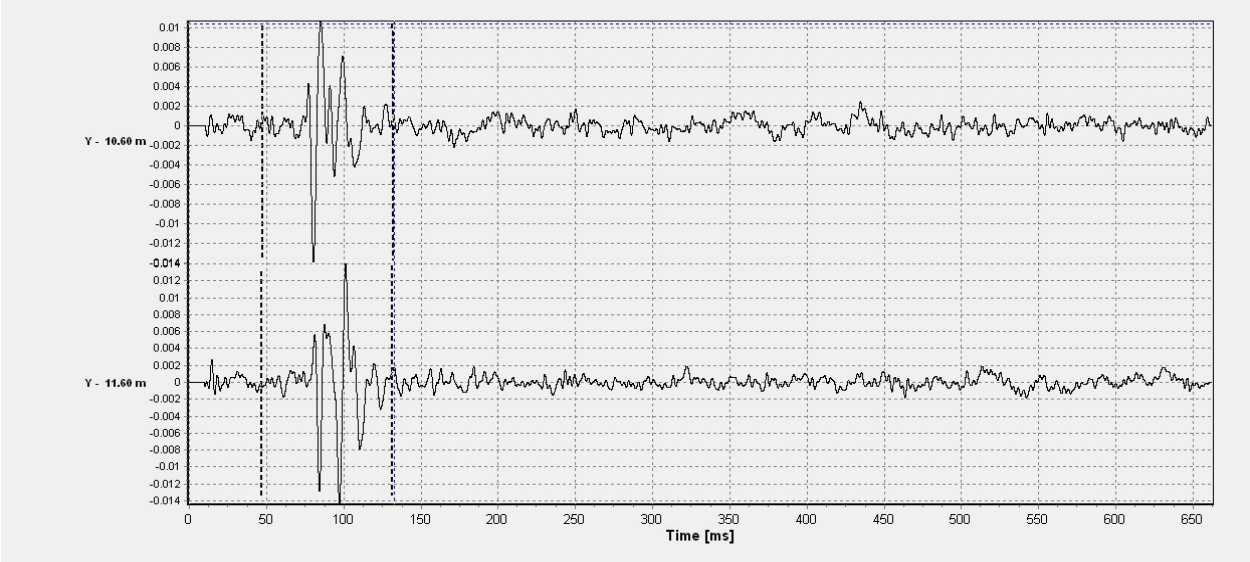

Figure 2: Low SNRs SCPT data sets acquired at depths 10.6 m and 11.6 m. The amplitudes are particle accelerations specified in m/s^2.

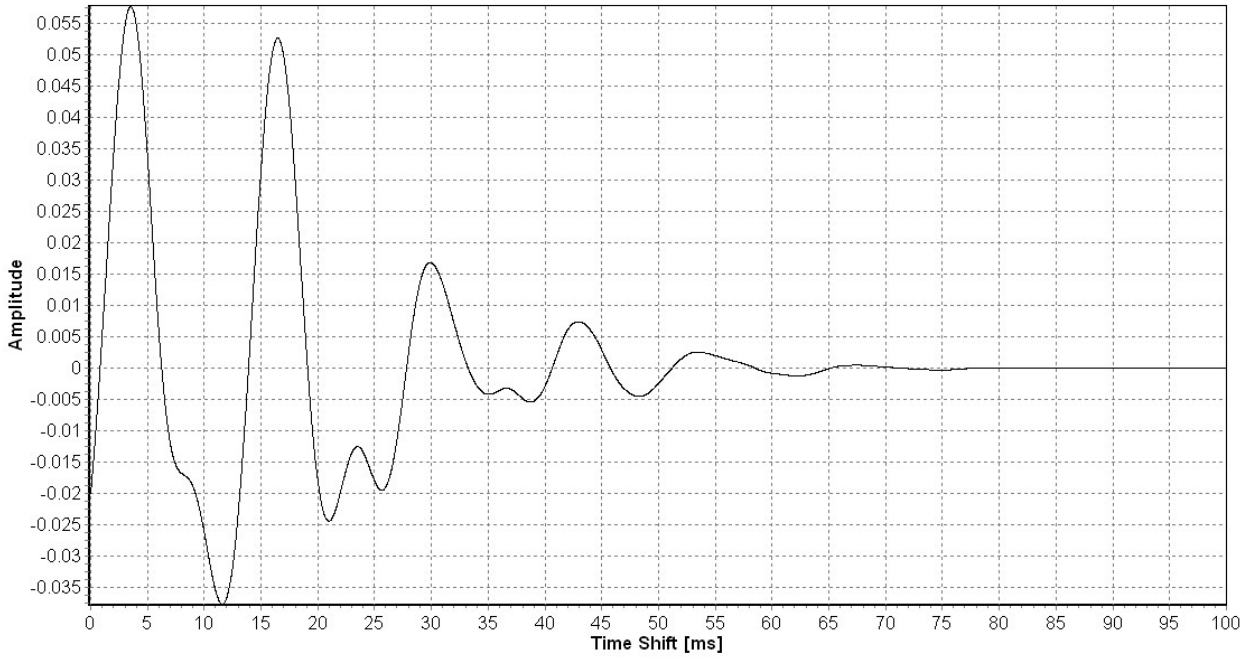

Figure 3: The cross correlation function for the data set illustrated in Fig. 2. Time window is set from 47 ms to 130 ms.

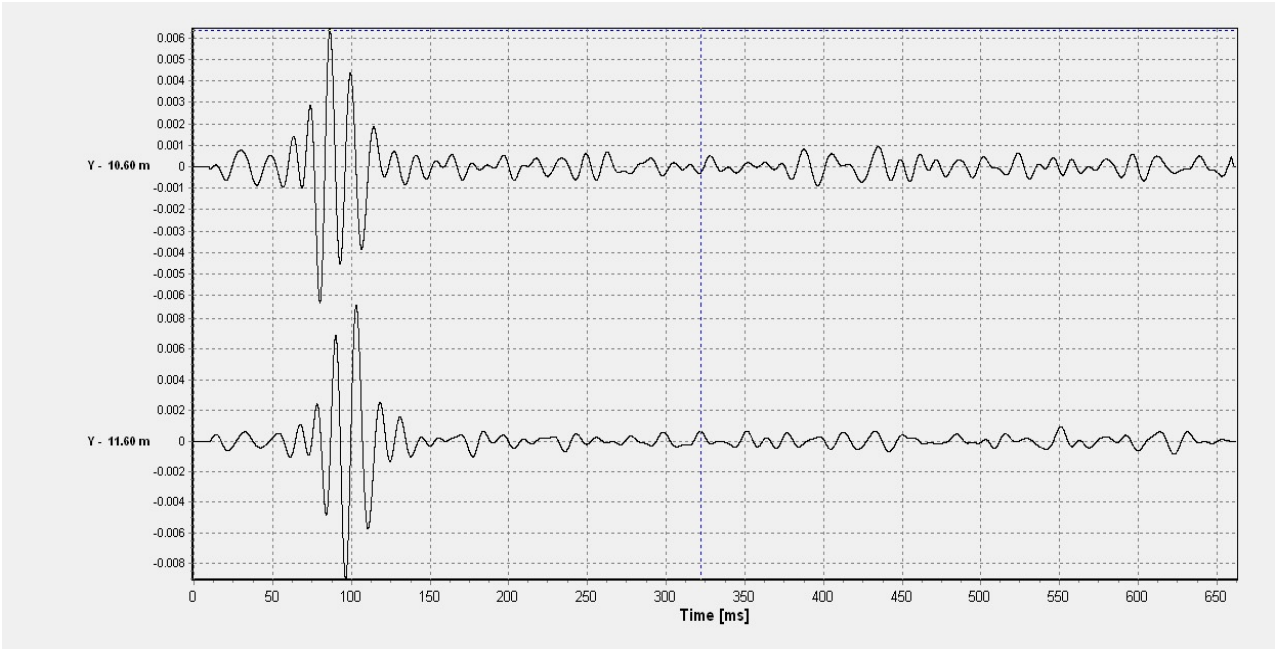

Figure 4: SCPT data set illustrated in Fig. 2 with a digital bandpass filter of 30 Hz to 100 Hz applied. The amplitudes are particle accelerations specified in m/s^2.

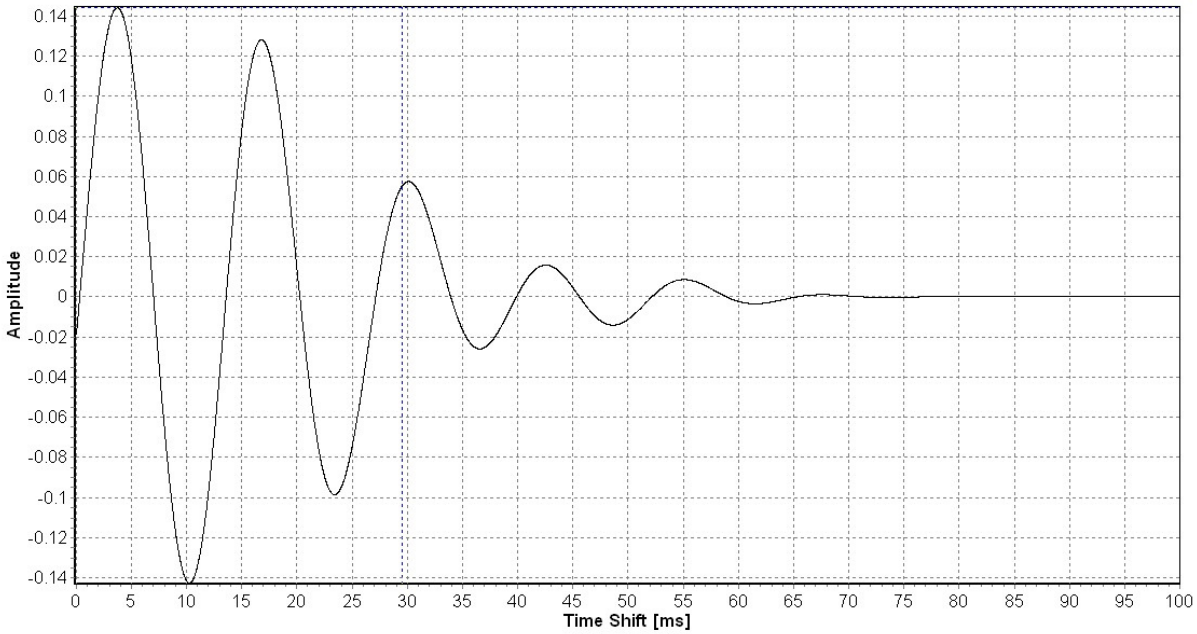

Figure 5: The cross correlation function for the data set illustrated in Fig. 4. Time window is set from 47 ms to 130 ms.

Information Set 2: Linearity Estimates from the Polarization Analysis

Theory

Seismic sources for DST are often designed to generate either predominantly P and SV waves or predominantly SH waves due to the fundamentally different behavior of these wave types at a boundary. When a P or SV wave strikes a boundary, four outgoing waves are generated (reflected P and SV waves as well as transmitted P and SV waves), while an SH wave will only generate reflected and transmitted SH waves data (Baziw, 2002; Aki and Richards, 2002; Shearer, 1999) thus simplifying the interpretation of the recorded seismic time series and making DST SH wave analysis preferred over SV wave analysis when determining *in-situ* low strain shear modulus values.

Another way to simplify the analysis of DST data sets is the use of relative large sensor-source radial offsets (Baziw and Verbeek, 2014c), as this significantly decreases near field amplitudes resulting in significantly higher Signal to Noise Ratios (SNRs) of the recorded seismic data, which in turn allows for more accurate near surface stratigraphy characterization. In addition, in case of SCPT this approach results in minimal recording of "rod" noise. Finally, large radial offsets improve the near surface characterization of the layer or depth under analysis due to the fact that the source wave refracts and travels within stratigraphic layers for a longer period of time. Obviously when applying larger radial sensor-source offsets the implementation of Fermat's Principle must be taken into account when analyzing the acquired seismic DST data (Baziw, 2002 and 2004a; Baziw and Verbeek, 2012 and 2014c; Aki and Richards, 2002; Shearer, 1999).

In DST investigations it is generally assumed that the stratigraphy under analysis is transversely isotropic (Baziw, 2004a; Aki and Richards, 2002) given the geological process of stratification. Shearer (1999) states that transverse isotropy (TI) is a particularly simple form of anisotropy, because velocities only vary with vertical incidence angle and not with azimuth. In addition, the two quasi-shear (qSH and qSV) wave polarizations correspond to SH and SV, and the qSH and qP/qSV systems can be treated separately.

The calculation of the incident angles of the particle motion of the source seismic wave allows the investigator to derive the full (three dimensional) seismic source waveform response. If the primary source wave is a P-wave the three-component time series, X(t), Y(t), and Z(t) can be rotated into the local ray path coordinate system with the longitudinal component in the compression wave (P) direction and two transverse components in the direction of the shear waves (SV and SH). In case of an SH source the X and Y axes responses can be rotated onto the full waveform SH-wave axis. This significantly simplifies the post-analysis, since a single full waveform response is analyzed instead of component responses on the X and Y axes.

Polarization Analysis (PA) is applied when rotating the acquired X(t), Y(t) and Z(t) seismic recordings onto the full waveform axis. In PA the full seismic waveform's angle of incident is determined using hodograms, and rectilinearity estimates are obtained by calculating the covariance matrix of the orthogonal X(t), Y(t) and Z(t) seismic trace recordings (Kanasewich, 1981; Baziw *et. al.*, 2004b). The analysis procedure can then be summarized as follows:

1. A time window is first applied to the seismic event of interest.

2. The X(t), Y(t), and Z(t) component seismic time series amplitudes are plotted against one another within this time window (to create hodograms).

3. Least squares straight line best fits are applied to the hodograms and the slopes of these straight lines provide angle of incidence information. With the latter the X(t), Y(t) and Z(t) seismic responses can then be rotated onto the full waveform. If SH(t) wave analysis is being carried out then only one Y(t) vs X(t) hodogram is required to obtain an angle of incidence estimate and subsequently the X(t) and Y(t) responses are rotated onto the SH(t) axis.

4. A covariance matrix is calculated for the X(t), Y(t) and Z(t) recordings over the hodogram time window specified (obviously in case of a SH wave analysis only one two dimensional covariance needs to be calculated for the X(t) and Y(t) axis recordings). This covariance matrix is defined as follows (using the notation of Kanasewich (1981):

$$\boldsymbol{V}_{xyz} = \begin{bmatrix} Var[X(t)] & Cov[X(t),Y(t)] & Cov[X(t),Z(t)] \\ Cov[Y(t),X(t)] & Var[Y(t)] & Cov[Y(t),Z(t)] \\ Cov[Z(t),X(t)] & Cov[Z(t),Y(t)] & Var[Z(t)] \end{bmatrix} \quad (3)$$

In (3) Var and Cov are abbreviations for variance and covariance, respectively. The Var of a variable (e.g., X(t)) is given as

$$Var[X(t)] = \frac{1}{N}\sum_{i=1}^{N}(X_i - \mu_x)^2 \tag{4}$$

where μ_x denotes the mean of the variable X(t).

The Cov of two variables (e.g., X(t) and Y(t)) in discrete form is given as

$$Cov[X(t), Y(t)] = \frac{1}{N}\sum_{i=1}^{N}(X_i - \mu_x)\big(Y_i - \mu_y\big) \tag{5}$$

An estimate of the rectilinearity of the particle motion over the specified hodogram time window is obtained by diagonalizing the covariance matrix ((3)) and subsequently calculating the ratio of the principal axis of the diagonalized matrix. A measure of the rectilinearity is referred to as linearity and it is calculated as follows:

$$F(\lambda_1, \lambda_2) = 1 - \left({\lambda_2}/{\lambda_1}\right) \tag{6}$$

where λ_1 and λ_2 denote the largest eigenvalue and next largest eigenvalue of the diagonalized covariance matrix, respectively. The linearity approaches unity when the rectilinearity is high ($\lambda_1 \gg \lambda_2$) and approaches zero when the rectilinearity is low ($\lambda_1 \approx \lambda_2$).

In DST interval velocity estimation it is desired to have data sets with linearity values near unity. This will be the case for seismic traces recorded in TI medium with minimal measurement noise, clean source waves, and no signal distortions (e.g., reflections). The more any of these aspects are present the lower the linearity value will be and low linearity values will also be obtained when shear-wave splitting or shear wave birefringence occur (Gibowicz and Kijko, 1994).

Shear-wave splitting (SWS) occurs when there is significant in-situ anisotropy as is the case with shear waves propagating in rocks containing cracks or ellipsoidal inclusions. Figure 6 (Gibowicz and Kijko, 1994) outlines the SWS phenomenon. A shear wave enters and propagates in a medium containing aligned cracks, and the shear wave component with motion or displacement normal to the crack travels more slowly (lower shear modulus) than the shear wave component with displacement parallel to the crack alignment. Consequently the two shear wave components will have different arrival times. The characteristic ellipsoid appears when obtaining the hodogram for these two SWS components. Although SWS splitting is rare in DST investigations, PA proves to be a powerful tool for identifying and characterizing significant in-situ anisotropy.

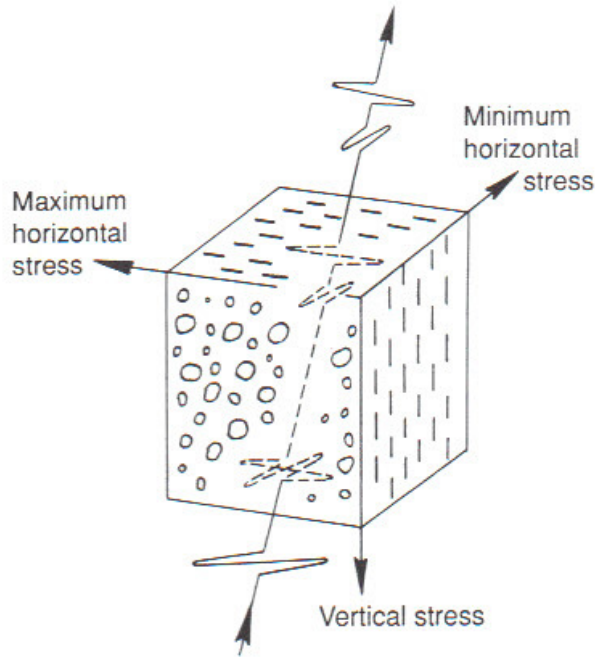

Figure 6: Illustration of shear-wave splitting in cracked rock (Gibowicz and Kijko (1994)).

Examples

To illustrate the concepts of PA, hodograms and rectilinearity two examples are given. The first example involves triaxial seismic data shown in Fig. 7 where the X, Y and Z responses from a SH source (after applying a low pass frequency filter of 140 Hz) have clearly high SNRs values: the peaks and troughs on the X and Y axis line up, and there are minimal recordings on the Z axis as would be expected for this kind of source. The hodogram plot for the time window of 50 ms to 80 ms is shown in Fig. 8 with the thick black bold line the best fit straight line (with a calculated linearity of 0.945). This clearly reflects a good quality seismic source recording with a high correlation between the X and Y axis and high directionality along an axis with an azimuth of approximately 13.5º. Please note that a relatively large time window (say 15 ms on either side of the first trough, or 50 to 80 ms) should be specified for the hodogram time window when assessing the data quality to account for erroneous outliers and residual measurement noise.

The second example involves another triaxial seismic trace recording shown in Fig 9, but in this case the peaks and troughs on the X, Y and Z do not line-up and the background noise (whether due to a poor source, vibrations within the testing vehicle upon impact of the SH wave sledge hammer, source wave reflection and/or other causes) has frequency components similar to the source wave making the isolation of the source wave with frequency filters a challenging tasks. The hodogram plot for the time window of 40 ms to 80 ms of this recording is shown in Fig. 10. The thick black bold line is again the best fit straight line, but obviously with a much lower calculated linearity (0.56) than in the previous example.

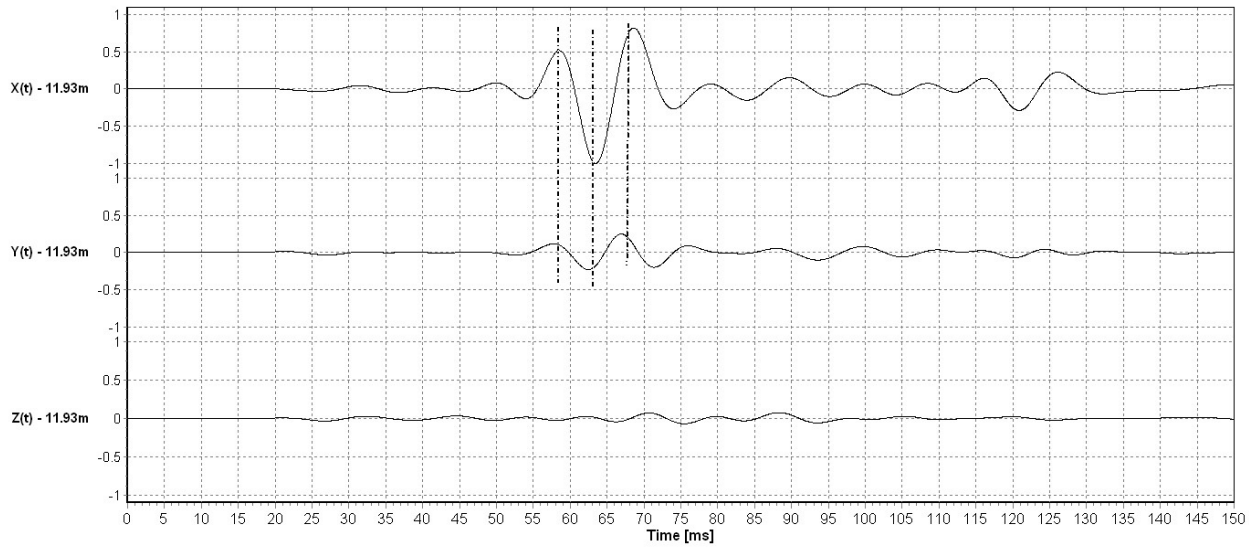

Figure 7: SH-wave responses on the X and Y axes where the peaks and troughs line-up in time giving high rectilinearity. Option *Normalize locally* implemented.

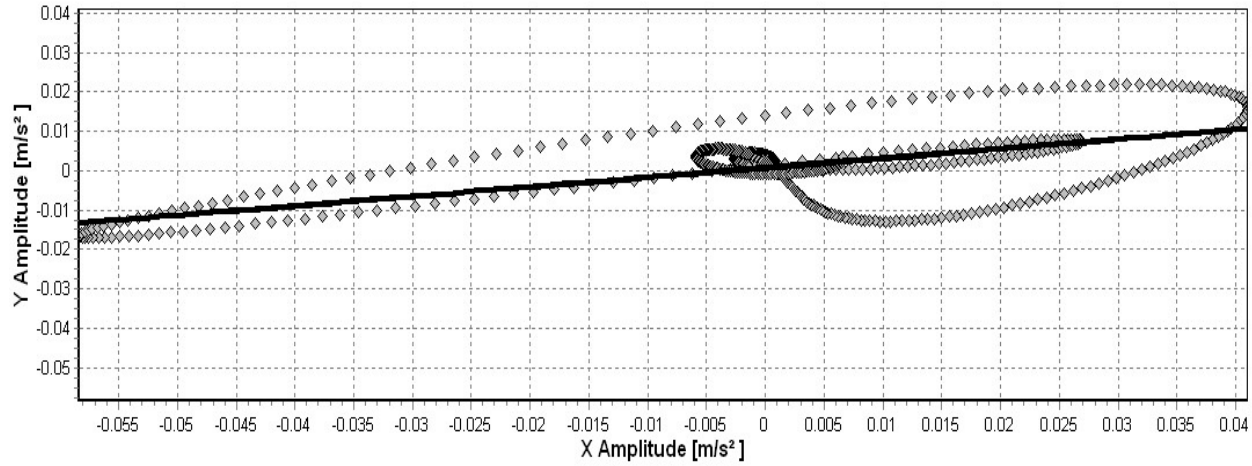

Figure 8: X(t) and Y(t) axes hodogram (time window = 50 ms to 80 ms) for seismic data illustrated in Fig. 7. The calculated linearity is 0.945 with an angle of incidence 13.5º. Thick black line is the linear least squares best fit.

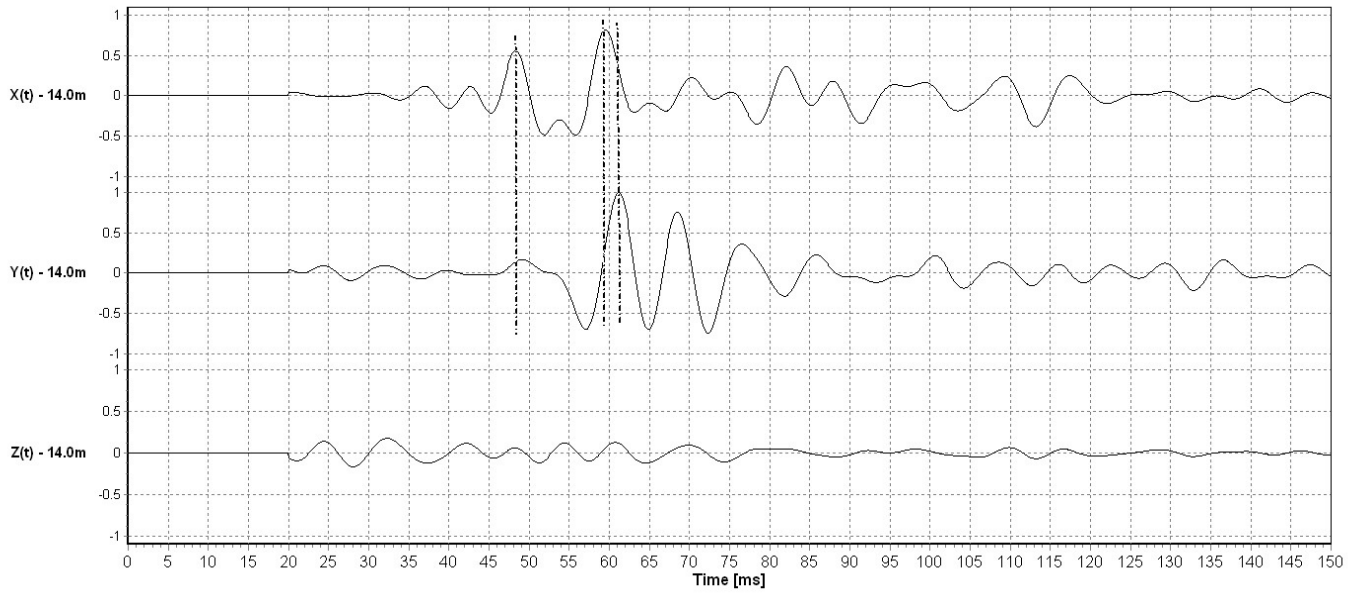

Figure 9: Poorly correlated SH-wave responses on the X and Y axes where the peaks and troughs do not line-up in time. Option *Normalize locally* implemented.

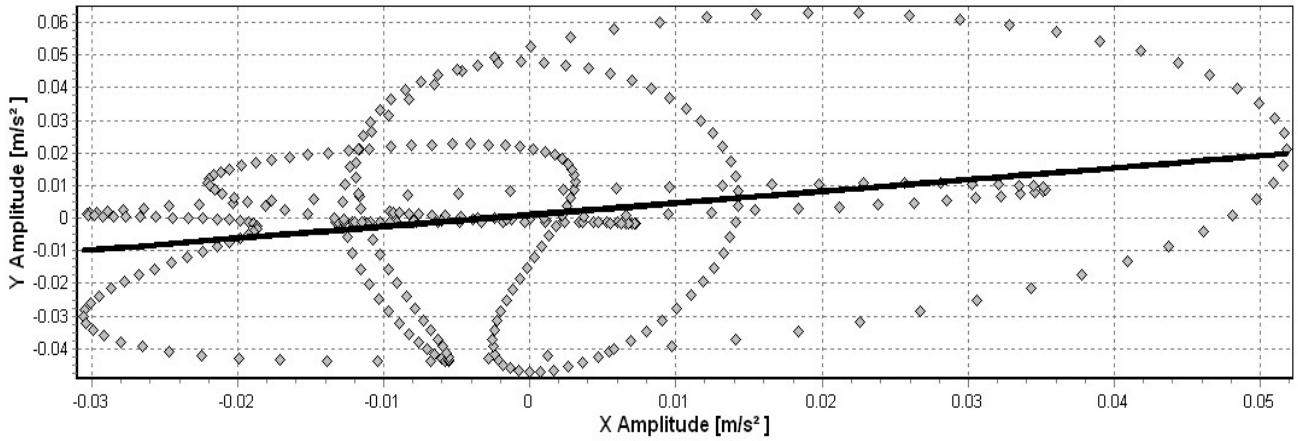

Figure 10: X(t) and Y(t) axes hodogram (time window = 40 ms to 80 ms) for seismic data illustrated in Fig. 9. The calculated linearity is 0.56. Thick black line is the linear least squares best fit.

Linearity Estimates from the Polarization Analysis vs Cross-Correlation Coefficient

An important characteristic of the linearity values calculated at a specific depth is that it is a completely independent assessment parameter from the CCC value, which was used as the first Information Set. It is possible to have data sets which have linearity values approaching unity and low CCC values, or sets with linearity and CCC values near unity, or with low linearity and low CCC values. This is illustrated in Fig. 11 (Kanasewich 1981):

- in Fig. 11(a) the linearity of the Y(t) vs X(t) data set approaches unity, but the CCC value is low;
- in Fig. 11(b) both the linearity and CCC value approach unity;
- in Figs. 11(c) and (d) both the linearity and CCC value are low.

However, just as the CCC value alone may provide an incorrect quality assessment, the linearity value may also be misleading. A real data example of this is given in Section 2.3.3 of this paper.

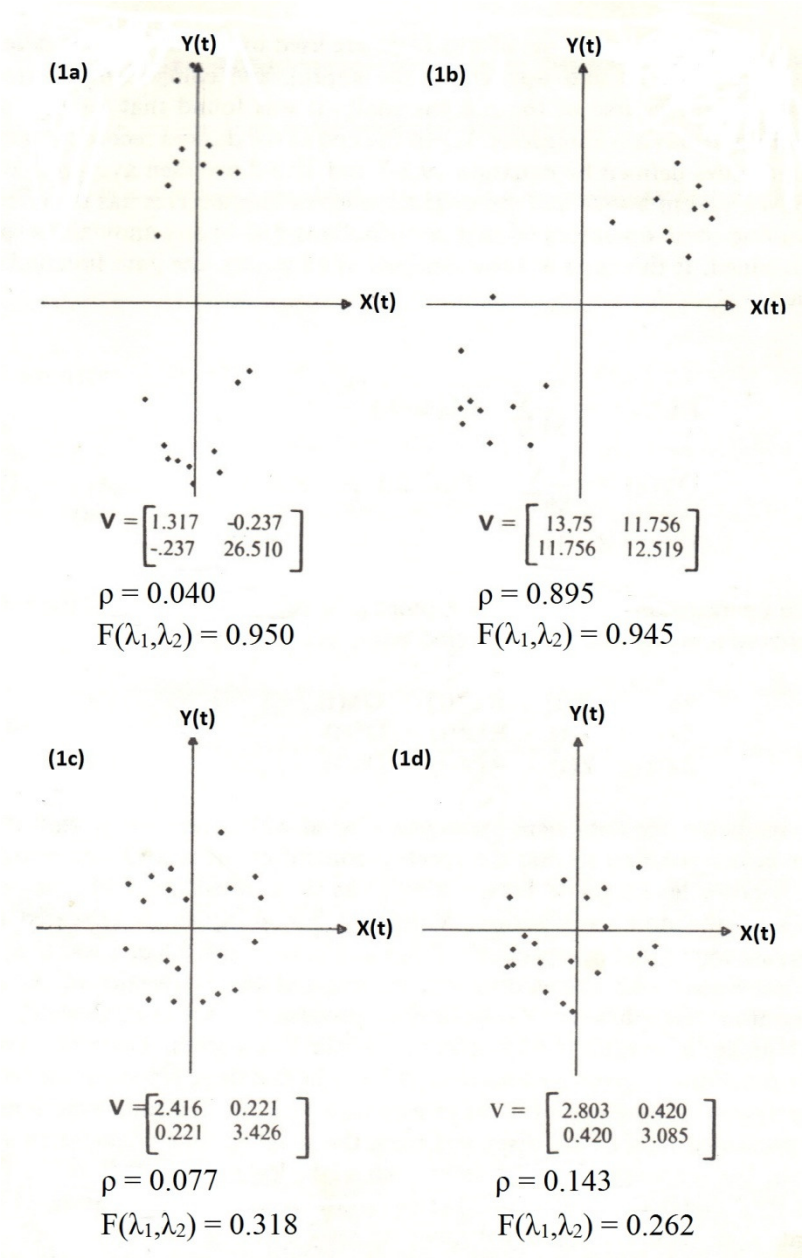

Figure 11: Examples of varying CCC and corresponding linearity values for Y(t) and X(t) data sets (after Kanasewich (1981)). (a) Low ρ and high F. (b) High ρ and high F. (c)-(d) Low ρ and low F.

Information Set 3: Signal Shape Parameter from Frequency Spectrum "Bell Curve" Fitting

Theory

The probability density of a normal (or Gaussian) distribution is given as

$$p(f|\mu,\sigma^2) = \frac{1}{\sigma\sqrt{2\pi}} e^{-\frac{(f-\mu)^2}{2\sigma^2}} \tag{7}$$

where μ denotes the mean or expectation of the distribution and σ denotes the standard deviation with variance σ^2. The area under the normal pdf curve is unity. Figure 12 illustrates example of normal pdfs for varying μ and σ^2 values. All the curves in Fig. 12 have the classical bell-shape. The pdf curve for the bell-curve approximation is given by (7) where f is the frequency, μ denotes the expected frequency and σ^2 is the estimated variance of the frequency spectrum.

Figure 13 illustrates a Berlage source wave (Baziw and Ulrych, 2006; Baziw and Verbeek, 2014 and 2016), which is commonly used within seismic signal processing for simulation purposes. The Berlage source wave is analytically defined as

$$w(t) = AH(t)t^n e^{-ht}\cos(2\pi f t + \emptyset) \tag{8}$$

where *H(t)* is the Heaviside unit step function [*H(t) = 0* for $t \leq 0$ and *H(t) = 1* for $t > 0$]. The amplitude modulation component is controlled by two factors: the exponential decay term *h* and the time exponent *n*. These parameters are considered to be nonnegative real constants. Figure 14 illustrates the frequency spectrum (solid black line) of the Berlage source wave shown in Fig. 13 with the normal pdf approximation shown as a dotted grey line, with μ = 69 Hz and σ = 32.5. As is evident from Fig. 14, the frequency spectrum of the simulated Berlage source wave closely matches that of a bell-shaped curve.

To incorporate the deviation of the source wave frequency spectrum from a desirable bell-shaped curve into the *IVC* the following process is proposed (Baziw and Verbeek, 2016):

1. Apply a digital zero-phase shift frequency filter (e.g., 130 Hz to 200 Hz Hz low pass frequency filter for SH recordings) to acquired seismic traces so that high frequency measurement noise is removed. Determine the component (x, Y or Z axis) which has the dominant response. This would be either the X or Y axis for SH source wave analysis.
2. Calculate frequency the spectrum (denote as *S(f)*)) for the axis which has the dominant response.

3. Force the area under *S(f)* to approach unity by uniformly modifying the amplitudes within *S(f)*. This step is outlined below by 9(a) and 9(b).

$$Area_{S(f)} = \Delta f \sum_{i+1}^{n} S(f)_i \tag{9a}$$

$$\sum_{i+1}^{n} S(f)_i = S(f)_i / Area_{s(f)} \tag{9b}$$

In 9(a), *Δf* denotes the frequency increment resolution.

4. Determine μ (dominant frequency), $p(\mu)$ (maximum spectral amplitude), and $\sigma = 1/(p(\mu) \sqrt{(2\pi)})$ utilizing an iterative forward modelling (IFM) technique such as the simplex method (Baziw, 2002 and 2011). In this IFM case the cost function to minimize is the RMS difference between the normalized area under *S(f)* and the derived area (using (7)) from a normal pdf which utilizes the currently estimated μ and σ values.

5. Calculate *p(f)* via (7) utilizing the IFM estimates μ and σ from Step 4.

6. Calculate $\epsilon_1 = \sum_{i+1}^{n} abs\big(S(f)_i - p(f)_i\big)$

7. Calculate $\epsilon_2 = \sum_{i+1}^{n} abs(S(f)_i)$

9. Signal Shape Parameter (*SSP*) component of the *IVC* is then calculated $SSP = 1 - \varepsilon_1/\varepsilon_2$

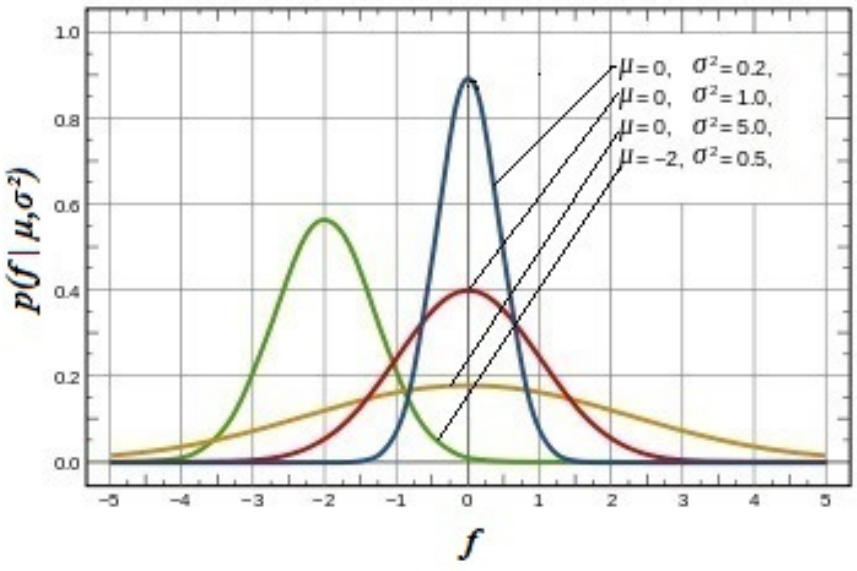

Figure 12: illustrates example of normal pdfs for varying μ and σ^2 values. (after, http://www.dplot.com/probability-scale.htm)

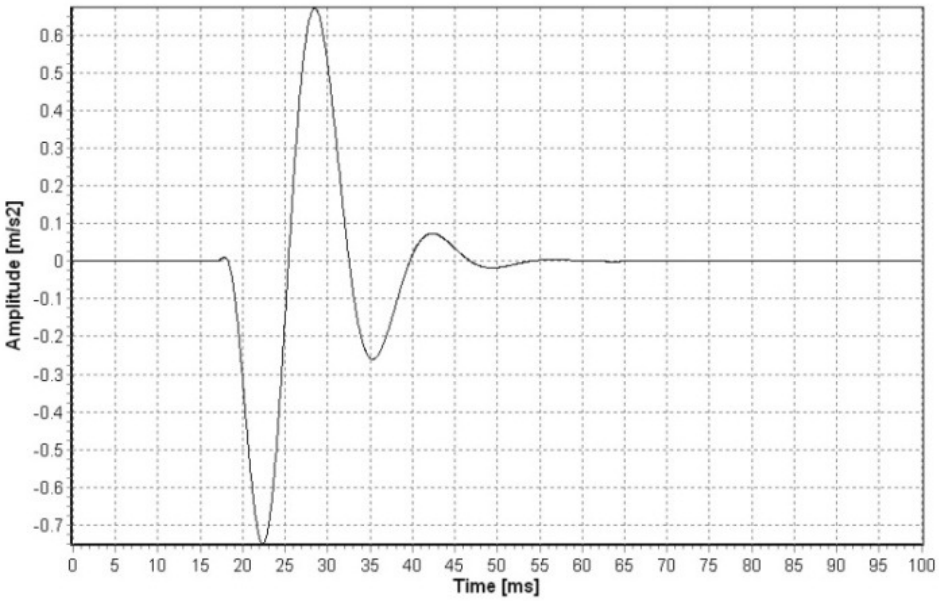

Figure 13: Berlage source wave with $f = 70\ Hz$, $n = 2$, $h = 270$ and $\phi = 40^{o}$ specified (Baziw and Verbeek, 2016).

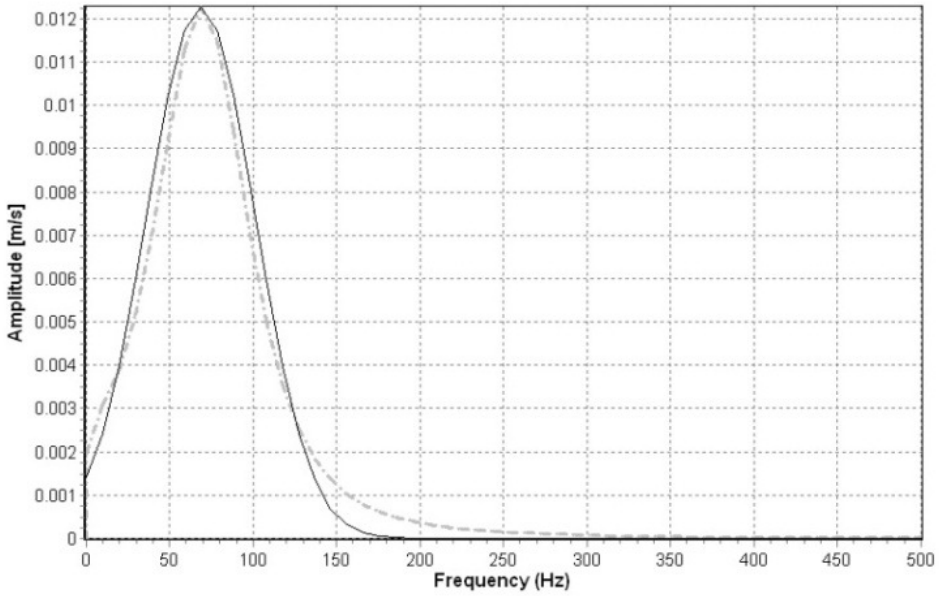

Figure 14. Frequency spectrum (solid black line) of Berlage source wave illustrated in Fig. 13 with the normal pdf approximation shown as a dotted grey line (Baziw and Verbeek, 2016).

Examples

High SNR SCPT data set

Figure 15 illustrates a real data example of a high SNR SH source wave SCPT trace acquired in Alberta, Canada. The triaxial data was acquired at a depth of 5m by fast response pcb accelerometers (5μs response time) with a bandwidth of 10 Hz to 10 KHz. The triaxial seismic data displayed in Fig. 15 had an option referred as *normalize locally* implemented, i.e. the displayed amplitudes of the X(t), Y(t), and Z(t) axes were normalized with respect to the absolute maximum value. This provides for a clear visual of the dominant X(t), Y(t) and Z(t) dominant responses. As is evident from Fig. 15, the dominant responses occur on the Y axis.

Using the filtered Y axis trace of Fig. 15 (150 Hz low pass filter applied) the frequency spectra were then calculated as outlined in Step 2. Figure 16 illustrates the Y axis frequency spectrum (solid black line) of triaxial source wave illustrated in Fig. 15 where the frequency spectrum amplitudes were uniformly modified so that the area under the curve was unity (Step 3).

The spectrum in Fig. 16 is then fed into the IFM portion of the bell-curve fitting algorithm that generated the optimal values of μ and σ of 91 Hz and 28.3, respectively were obtained. Figure 16 illustrates the estimated normalized pdf superimposed upon the unity area frequency spectrum. Using Steps 6, 7 and 8 generated the following result: $\varepsilon_1 = 0.193$, $\varepsilon_2 = 1.632$, and SSP = 0.882 were obtained. This high SSP value indicates a high quality seismic trace, which is confirmed by the linearity value for this trace of 0.925.

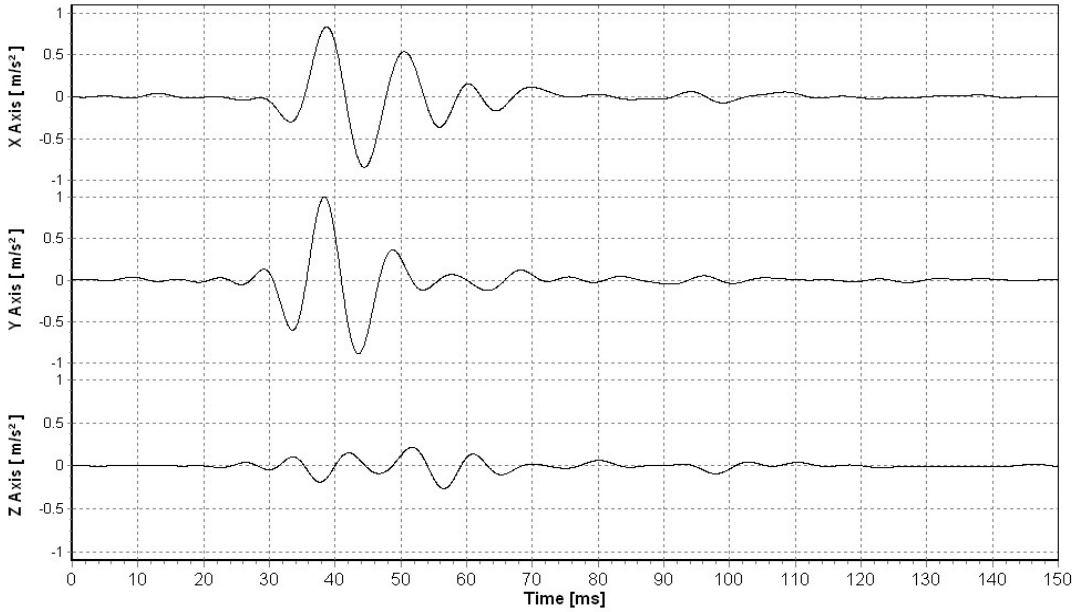

Figure 15: Filtered (150 HZ low pass frequency filter) high SNR SCPT triaxial accelereometer data set.

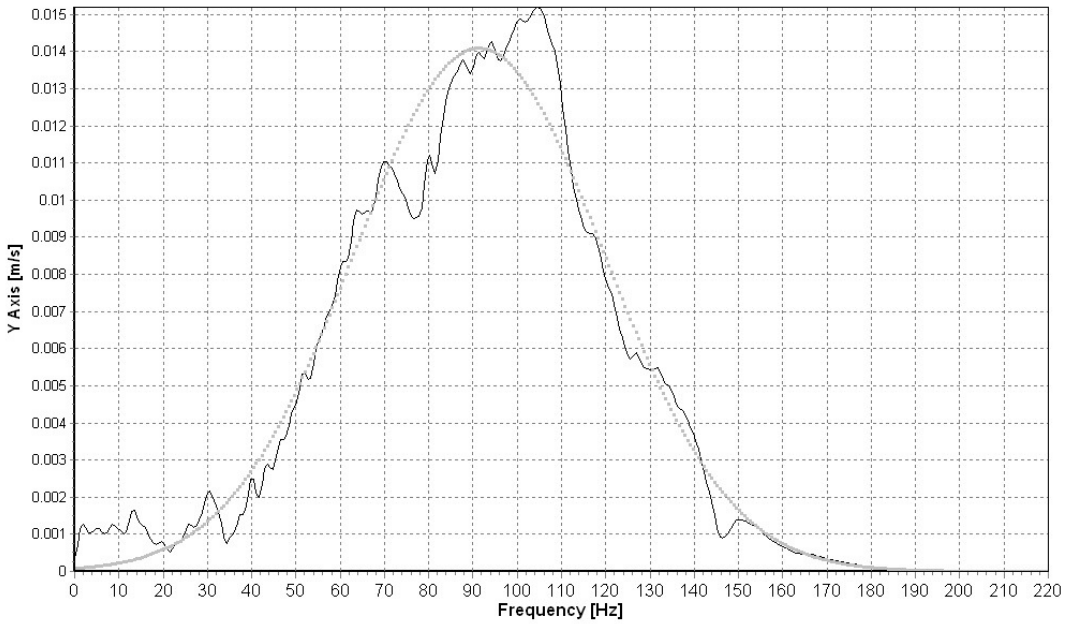

Figure 16: Y axis frequency spectrum (solid black line) of triaxial source wave illustrated in Fig. 15 with the normal pdf approximation shown as a dotted grey line.

Low SNR SCPT data set

Figure 17 illustrates another real data example (once again normalized locally) where we have low SNR SH source wave SCPT traces (only X and Y axis responses illustrated) acquired in New Zealand, using the same pcb accelerometers that were used in the previous example. The traces illustrated in Fig. 17 have had a 150 Hz low pass digital frequency filter applied. The Y axis has the dominant responses. The frequency spectrum of the Y axis trace was calculated from the filtered trace illustrated in Fig. 17. Figure 18 illustrates the Y axis frequency spectrum (solid black line) of the seismic time series illustrated in Fig. 17 where the frequency spectrum amplitudes were uniformly modified so that the area under the curve was unity (Step 3).

Using the same process as described for the previous example the following results were obtained: μ = 88.2 Hz, σ = 39.1, ε_1 = 0.896, ε_2 = 1.814, and *SSP* = 0.506. The value of *SSP* = 0.506 identifies a low quality seismic trace. As could be expected the linearity value obtained for this trace is also lower (0.417).

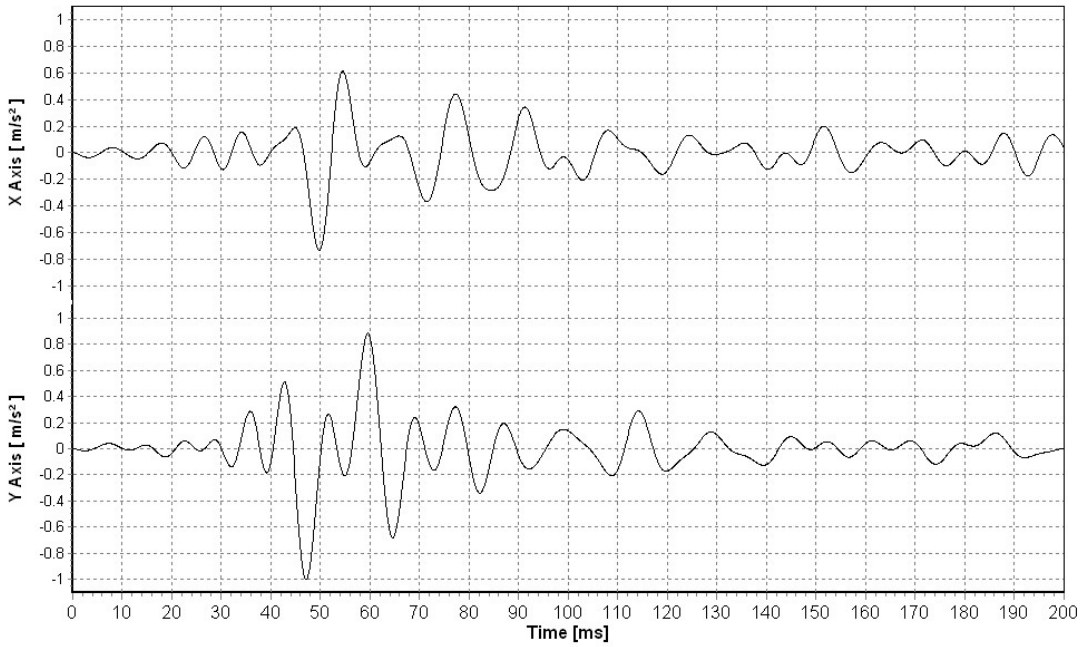

Figure 17: Filtered (150 Hz low pass frequency filter) low SNR SCPT accelereometer data set. X and Y axis responses illustrated.

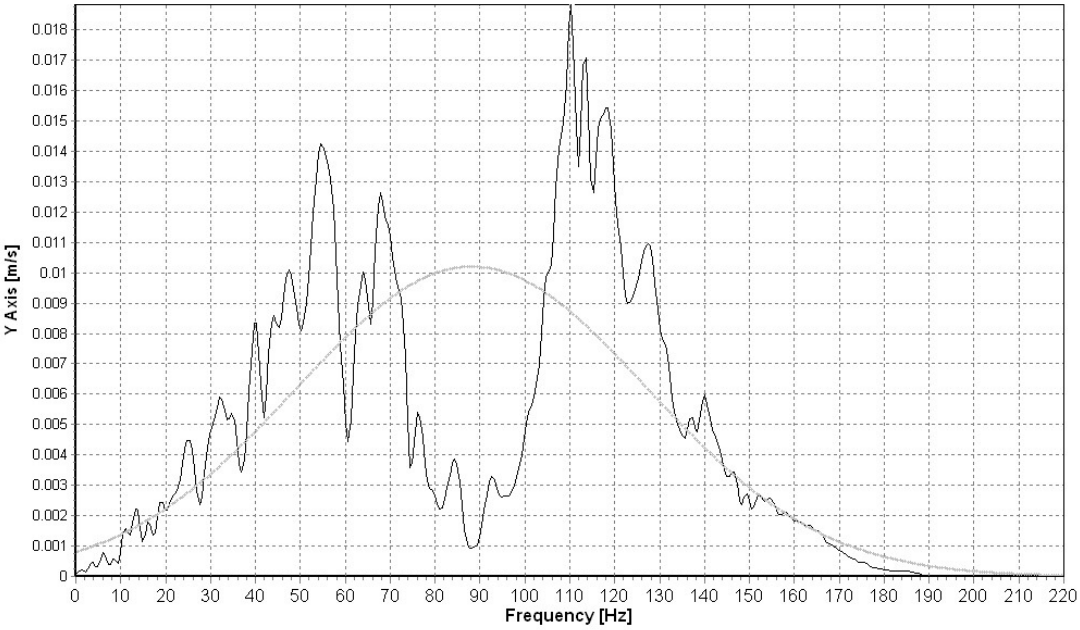

Figure 18: Y axis frequency spectrum (solid black line) of Y axis time series illustrated in Fig. 17 with the normal pdf approximation shown as a dotted grey line.

SSP vs. Linearity Estimates vs Cross-Correlation Coefficient

It shall be obvious that the SSP is completely independent from the linearity estimates and the CCC. This has proven very advantageous in case the seismic traces contain correlated noise with relatively high linearity. Without the SSP component it would be difficult, if not impossible to identify the low IVC data sets (during batch processing) and carry out subsequent additional signal enhancement. Figure 19 illustrates SCPT X(t) and Y(t) seismic traces acquired in New Zealand at depths of 31m and 32m (filtered with a 20 Hz to 130 Hz bandpass digital frequency filter) . These traces clearly have low SNRs, but the linearity values are determined to be the relatively high values of 0.78 and 0.79, respectively, with a CCC value of 0.85. At the same time the SPP values for the traces at 31m and 32m were calculated to be relatively low (0.51 and 0.49, respectively), which clearly demonstrates that it is possible to have data sets with relatively high linearity and CCC values and yet low SSP values.

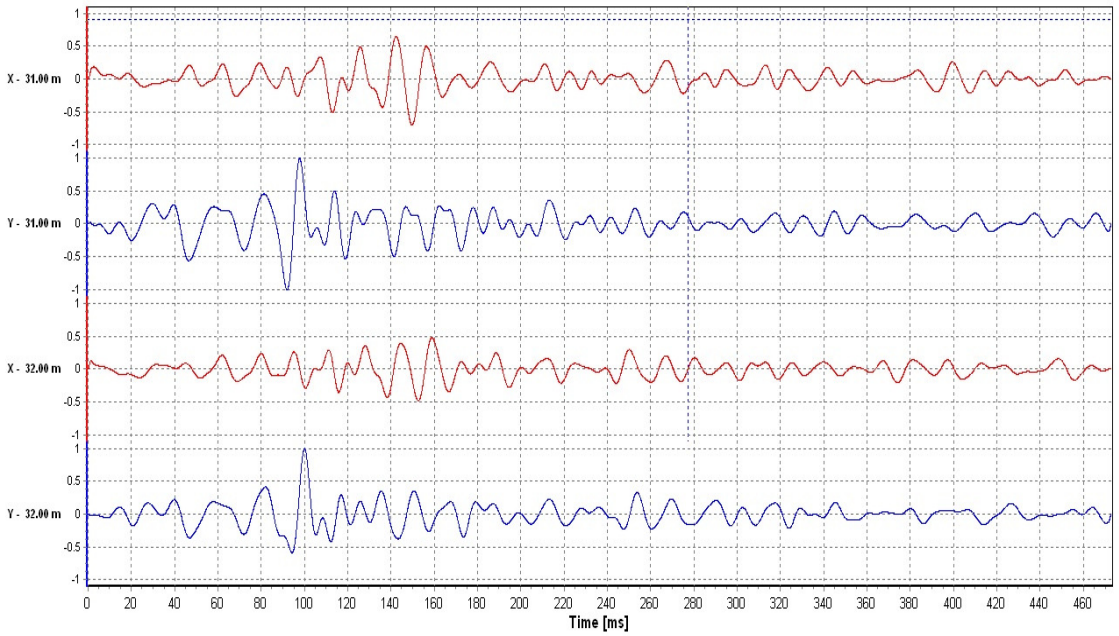

Figure 19: SCPT X(t) and Y(t) axes filtered (20 Hz to 130 Hz) responses illustrating DST data sets with relatively high CCC and linearity values and corresponding low SSP values.

Interval Velocity Classification Methodology

Theory

To overcome the previously outlined limitations of the CCC, PA linearity and SSP estimates are incorporated into the Interval Velocity Classification for the quality assessment of the estimated interval velocities in DST using the following equation:

$$IVC = 0.4 \times CCC + 0.18 \times (L_1 + L_2) + 0.12 \times (SSP_1 + SSP_2) \quad (10)$$

In (10) we have a DST investigation where traces where acquired at the two successive depths of depth1 and depth2 (where depth2 > depth1) with

CCC - denotes the cross correlation coefficient between the full waveforms obtained at depth1 and depth2.

L_1 - linearity value for seismic traces acquired at depth 1

L_2 - linearity value for seismic traces acquired at depth 2

SSP_1 - signal shape parameter for seismic traces acquired at depth 1

SSP_2 - signal shape parameter for seismic traces acquired at depth 2

This value is then converted into a grade ranging from *A* to *F* as shown in Table 1, where A is highly desirable and *F* is unusable. While the proposed classification is based on a re-evaluation of many data sets previously processed (from over 40 different sites around the world, covering over 4000 seismic traces) it is likely it will be refined (through adjustments of the constants in (10) and/or adding additional parameters) in the future as it is applied on a routine basis for new data sets. Based on the authors' experience the IVC value is automatically set to D (if not already set to D or F) when Linearity < 0.7, SSP < 0.6 or CCC < 0.7.

INTERVAL VELOCITY CLASSIFICATION IMPLEMENTATION AND PERFORMANCE RESULTS

Typically DST data set are processed in batch mode where all the seismic traces from a given source and profile are processed automatically by implementing the following sequential steps (Baziw, 1993, 2002 and 2004a; Baziw and Verbeek, 2012 and 2014) :

1. Apply zero phase shift digital filters to increase SNRs of acquired traces.
2. Implement IVC algorithm and ascertain quality of acquired seismic traces.
3. If acceptable IVC values (A to C) obtained, then cross-correlate the filtered and sequentially (depth) acquired traces so that relative arrivals can be obtained. True arrivals are then derived based upon a user supplied reference arrival time.
4. The true arrival times are feed into an algorithm which takes Fermat's Principle and ray path refraction into account.

5. For SH analysis, two sets of independent interval velocities are obtained from source waves polarized on both the Right Side (RS) and the Left Side (LS) of the downhole seismic probe (Campanella, *et. al*, 1986).
6. The right side and left side interval velocities are compared.

In the above analysis process, DST seismic traces with low IVC values (D or F) should not be processed in a batch mode; instead the investigator should evaluate the traces in a very deliberate manner through more aggressive digital filters, individual Polarization Analysis for linearity assessment (e.g., specify smaller time window), utilization of dominant axis responses rather than calculated full waveforms, visually obtained arrival times using first breaks and/or dominant peaks or trough, or in extreme cases even deciding not to use traces at a particular depth for interval velocity estimation.
As more experience is gained with this approach the authors hope that more specific guidance regarding the most appropriate analysis approach can be derived from the individual parameters.

Examples

The first DST data set (the so-called SCPT1) was acquired during a SCPT at a site in New Zealand by Perry Geotech Ltd. The data was obtained at a coastal site underlain by sands deposited by Holocene coastal processes. The SH source waves at this site were generated with a pendulum sledge hammer horizontally impacting point source steel beams located underneath the outriggers (2.3 meters from the center of the rod string) and an electrical contact trigger. Figure 20 illustrates Perry Geotech's typical SCPT site setup. In Fig. 20, the LS and RS SH source wave pendulum hammers which have a radial offset of 2.3 m from the downhole seismic probe are illustrated. Two stacked SH source waves were generated for each depth increment, with data acquisition starting at 2 m and going down to 19 m. Two seismic data sets were acquired from right and left side polarized SH source waves.

Table 1. Interval Velocity Classification and Description

IVC Numeric Value (i.e., (10)) [0-1]	ÎVC Rank [A-F]	IVC Description
0.9 to 1.0	A	very good to good
0.8 to 0.9	B	good to acceptable
0.7 to 0.8	C	acceptable to questionable
0.65 to 0.7	D	questionable to unacceptable
< 0.65	F	unacceptable

Figure 20: Perry Geotech Ltd. of Tauranga New Zealand SCPT site setup. The LS and RS SH source wave pendulum hammers which have a radial offset of 2.3 m from the downhole seismic probe are illustrated.

Figure 21 illustrates the Left Side (LS) unfiltered VSP *normalized locally* X(t) and Y(t) axes responses for depths between 2m and 19m. Figure 22 outlines the full waveform estimates after application of a digital bandpass filter of 20 Hz to 130 Hz, PA and source wave windowing on the seismic data illustrated in Fig. 21. Figures 23 and 24 show the same for data from the Right Side (RS). Table 2 lists the RS and LS IVC values and the corresponding Linearity, SSP and CCC values for each depth increment. As outlined in Table 2 the IVC values are very high (B and A) and the investigator can have high confidence in the subsequently estimated DST interval velocities. Table 3 outlines the estimated DST interval velocities where there is very high correlation between the LS and RS estimates, as would be expected for estimated interval velocities with high IVC values and TI medium.

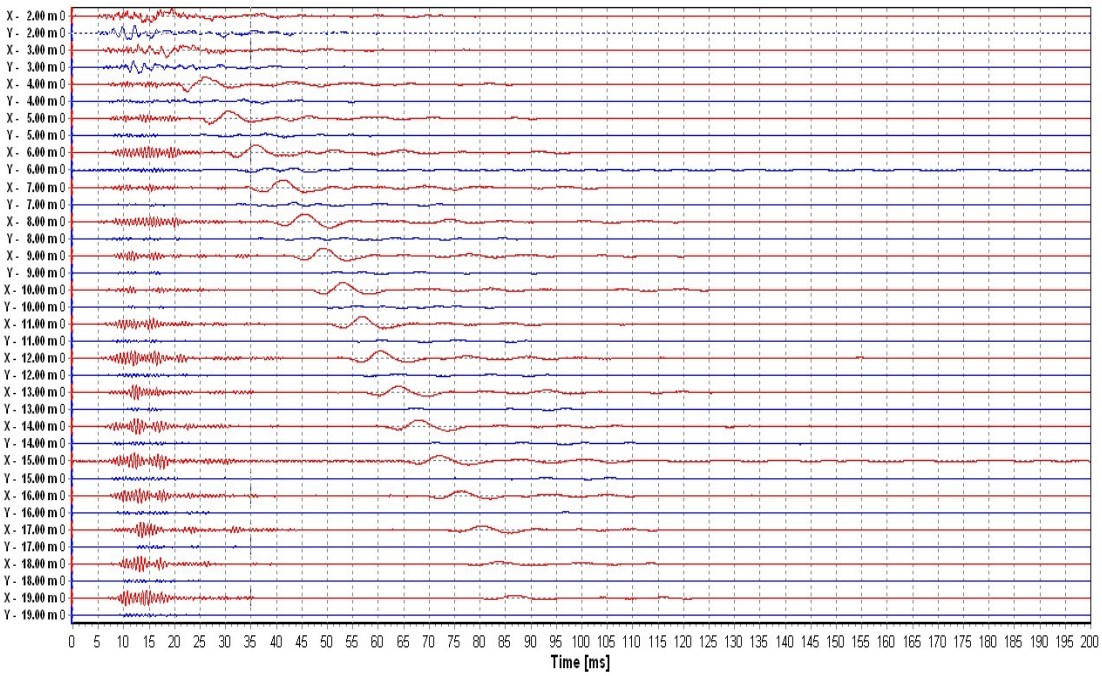

Figure 21: Site SCPT1 LS X(t) and Y(t) axes unfiltered. Option *normalize locally* implemented.

Table 2. Right Side and Left Side Interval Velocity Classifications for SCPT Site SCPT1

Left Side IVC					Right Side IVC			
Depth [m]	Linearity [0-1]	SSP [0-1]	CCC [0-1]	IVC [A-F]	Linearity [0-1]	SSP [0-1]	CCC [0-1]	IVC [A-F]
2	0.90	0.81	N/A	N/A	0.82	0.70	N/A	N/A
3	0.90	0.76	0.97	A	0.78	0.74	0.93	B
4	0.94	0.76	0.97	A	0.89	0.70	0.98	B
5	0.94	0.75	0.99	A	0.89	0.73	0.98	B
6	0.94	0.76	0.98	A	0.87	0.74	0.97	B
7	0.94	0.77	0.99	A	0.90	0.73	0.98	B
8	0.94	0.84	0.99	A	0.92	0.76	0.99	A
9	0.95	0.78	0.99	A	0.92	0.78	0.99	A
10	0.95	0.77	0.99	A	0.91	0.78	0.99	A
11	0.94	0.79	0.98	A	0.91	0.81	0.99	A
12	0.94	0.79	0.98	A	0.90	0.73	0.97	A
13	0.93	0.82	0.98	A	0.92	0.72	0.98	B
14	0.94	0.81	0.96	A	0.92	0.80	0.96	A
15	0.94	0.80	0.94	A	0.93	0.71	0.95	B
16	0.94	0.78	0.92	A	0.94	0.71	0.94	B
17	0.94	0.79	0.98	A	0.94	0.80	0.95	A
18	0.94	0.78	0.96	A	0.94	0.67	0.88	B
19	0.93	0.78	0.97	A	0.93	0.71	0.95	B

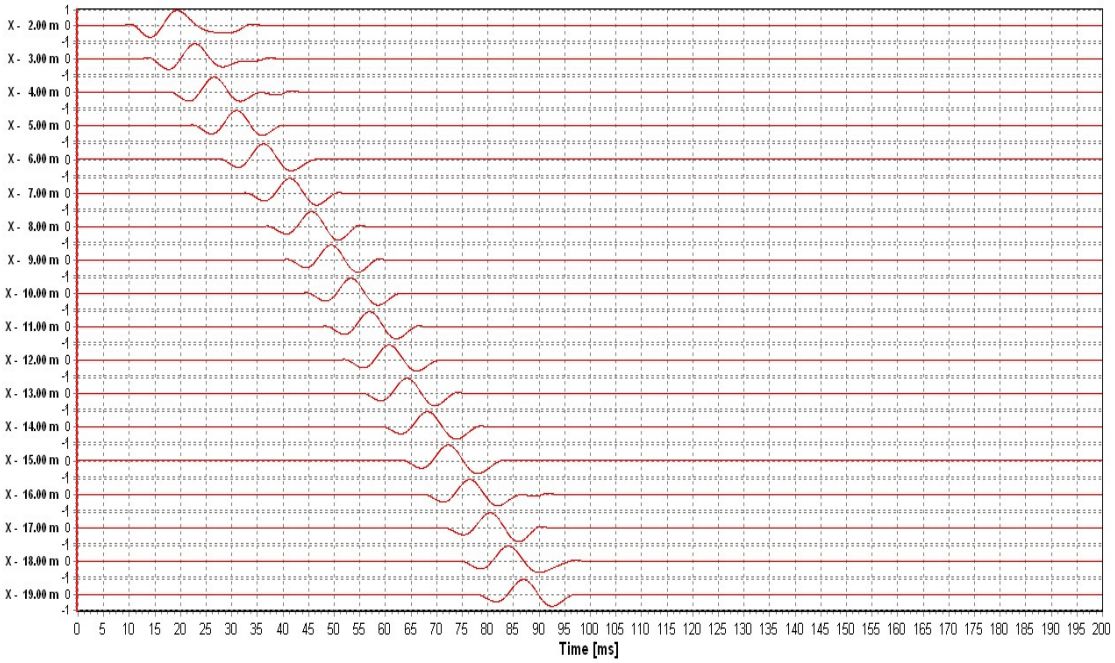

Figure 22: After application of a digital bandpass filter of 20 Hz to 130 Hz, PA and source wave windowing on the seismic data illustrated in Fig. 21. The LS full waveform responses are displayed.

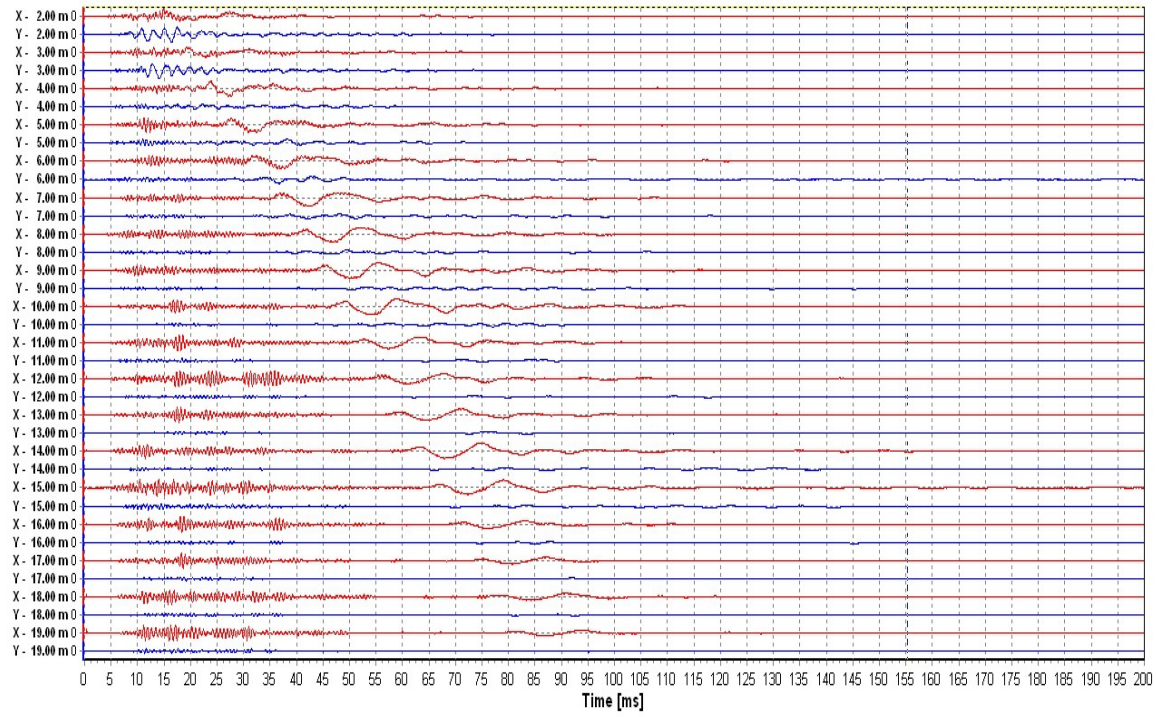

Figure 23: Site SCPT1 RS X(t) and Y(t) axes unfiltered. Option *normalize locally* implemented.

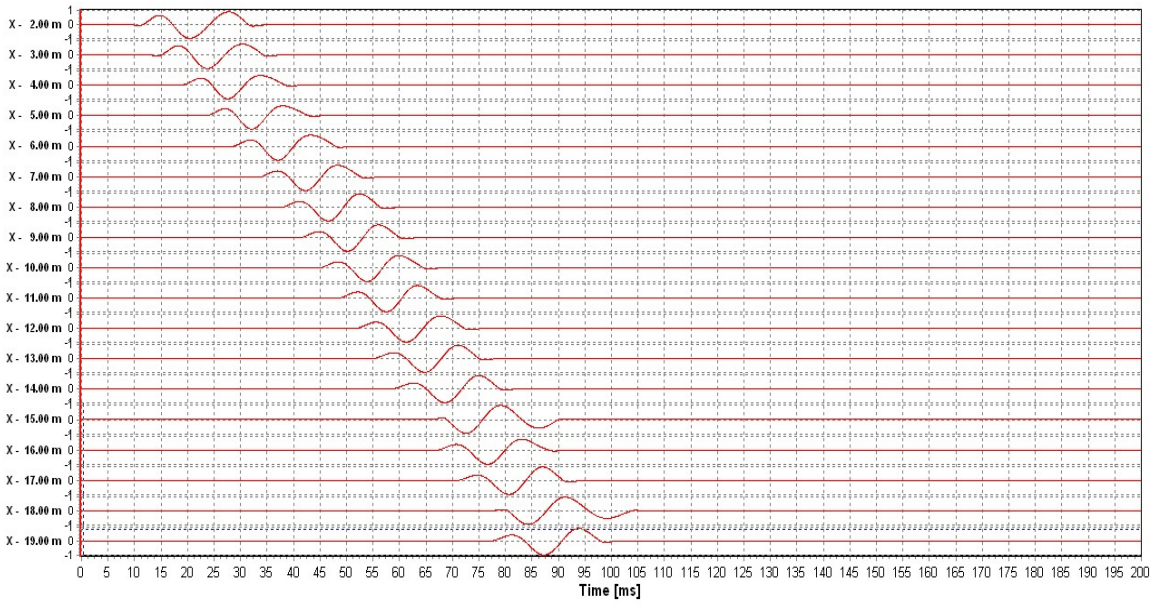

Figure 24: After application of a digital bandpass filter of 20 Hz to 130 Hz, PA and source wave windowing on the seismic data illustrated in Fig. 23. The right side full waveform responses are displayed.

Table 3. Right Side (RS) and Left Side (LS) Interval Velocity Estimates for SCPT Site SCPT1

Depth [m]	LS Interval Velocity [m/s]	RS Interval Velocity [m/s]	Avg. Interval Velocity [m/s]	Spread
0-2.0	217.7	218.1	217.9	0%
2.0-3.0	221.1	224.7	222.9	1%
3.0-4.0	222.5	218.2	220.4	1%
4.0-5.0	206.2	203.5	204.9	1%
5.0-6.0	177.5	188.7	183.1	3%
6.0-7.0	188.6	186.9	187.8	0%
7.0-8.0	225	227.6	226.3	1%
8.0-9.0	247.9	259.7	253.8	2%
9.0-10.0	246.1	255.3	250.7	2%
10.0-11.0	267.4	271	269.2	1%
11.0-12.0	254.1	246.2	250.2	2%
12.0-13.0	281.6	292.4	287.0	2%
13.0-14.0	242.4	254.6	248.5	2%
14.0-15.0	240.4	242.6	241.5	0%
15.0-16.0	239.1	239.1	239.1	0%
16.0-17.0	250.2	254.7	252.5	1%
17.0-18.0	262.2	246.1	254.2	3%
18.0-19.0	354	359.4	356.7	1%

The spread is defined as ½ x (LS Interval Velocity – RS Interval Velocity)/Avg. Interval Velocity

The second DST data set (the so-called SCPT2) was also acquired by Perry Geotech Ltd. The data was once again obtained at a coastal site underlain by sands deposited by Holocene coastal processes using the same set-up as described for the previous data set. Table 4 outlines the derived LS and RS IVCs values for the seismic data acquired at this site. At various depths the IVC values clearly indicated that corrective action is required. The occurrence of low IVC values on the left side is due to the corresponding low SSP values (< 0.6) occurring at depths 15m, 20m, 22m, 23m, 24m due to the "ringing" outside the dominant source responses. This "ringing" is illustrated in Fig. 25 where the X(t) and Y(t) axis responses are filtered with a 20 Hz to 130 Hz bandpass filter. The "ringing" may be due to source wave reflections or poor source waves generation. In Fig. 25 it is evident that there are strong responses on both the X and Y axes. Figure 26 illustrates the frequency spectrum (light grey trace) and corresponding "Bell-Shape" best fit (dark black trace) for the filtered seismic trace recorded at 22m (X axis dominant response illustrated in Fig. 25). The corresponding SSP value is 0.55. Low SSP values were addressed by applying a time windowing algorithm which significantly reduced any outlier responses. Figure 27 illustrates the frequency spectrum (light grey trace) and corresponding "Bell-Shape" best fit (dark black trace) for the filtered trace recorded at 22m with a time window applied so that the dominant source wave pulse is isolated. The corresponding SSP value has been increased to 0.821. Figure 28 illustrates the left side full waveform responses after appropriate filtering applied.

The RS IVC values outlined in Table 4 are generally reasonable, but they also indicate the need for some corrective action. The low IVC values at depths 2m and 3m are due to the associated low linearity values. It was decided to use the Y axes responses at these depths due to the fact that they were the dominant responses and had lower SNRs compared to the X axis responses. The low IVC values between 14m to 15m and 15m to 16m are due to the low SSP value at 15m, which was addressed similar to the LS low SSP by applying a time windowing algorithm. Figure 29 illustrates the RS full waveform responses after appropriate filtering applied. Table 5 outlines the subsequently estimated DST interval velocities where there is very high correlation between the LS and RS estimates, despite the poorer data quality as the components of the IVC technique provided valuable guidance for the data analysis process.

Table 4. Right Side and Left Interval Velocity Classifications for SCPT Site SCPT2

Left Side IVC					Right Side IVC			
Depth [m]	Linearity [0-1]	SSP [0-1]	CCC [0-1]	IVC [A-F]	Linearity [0-1]	SSP [0-1]	CCC [0-1]	IVC [A-F]
2	0.39	0.64	0	N/A	0.79	0.64	N/A	N/A
3	0.57	0.65	0.90	D	0.86	0.73	0.87	B
4	0.87	0.63	0.94	D	0.81	0.72	0.95	B
5	0.89	0.77	0.94	B	0.81	0.82	0.94	B
6	0.84	0.76	0.96	B	0.78	0.74	0.94	B
7	0.91	0.72	0.97	B	0.75	0.72	0.95	B
8	0.93	0.73	0.97	B	0.77	0.72	0.99	B
9	0.88	0.68	0.97	B	0.81	0.73	0.97	B
10	0.87	0.70	0.99	B	0.88	0.66	0.99	B
11	0.85	0.72	0.97	B	0.89	0.68	0.97	B
12	0.77	0.65	0.96	B	0.88	0.66	0.97	B
13	0.80	0.66	0.97	B	0.87	0.67	0.98	B
14	0.84	0.69	0.95	B	0.86	0.66	0.97	B
15	0.85	0.57	0.89	D	0.81	0.59	0.93	D
16	0.85	0.67	0.83	D	0.85	0.61	0.86	D
17	0.85	0.69	0.87	B	0.87	0.63	0.88	B
18	0.88	0.71	0.97	B	0.84	0.60	0.94	B
19	0.89	0.67	0.97	B	0.80	0.63	0.98	B
20	0.90	0.69	0.98	B	0.75	0.58	0.98	D
21	0.89	0.70	0.99	B	0.75	0.83	0.94	D
22	0.87	0.68	0.99	B	0.83	0.55	0.87	D
23	0.88	0.70	0.98	B	0.84	0.55	0.97	D
24	0.88	0.70	0.98	B	0.86	0.59	0.98	D

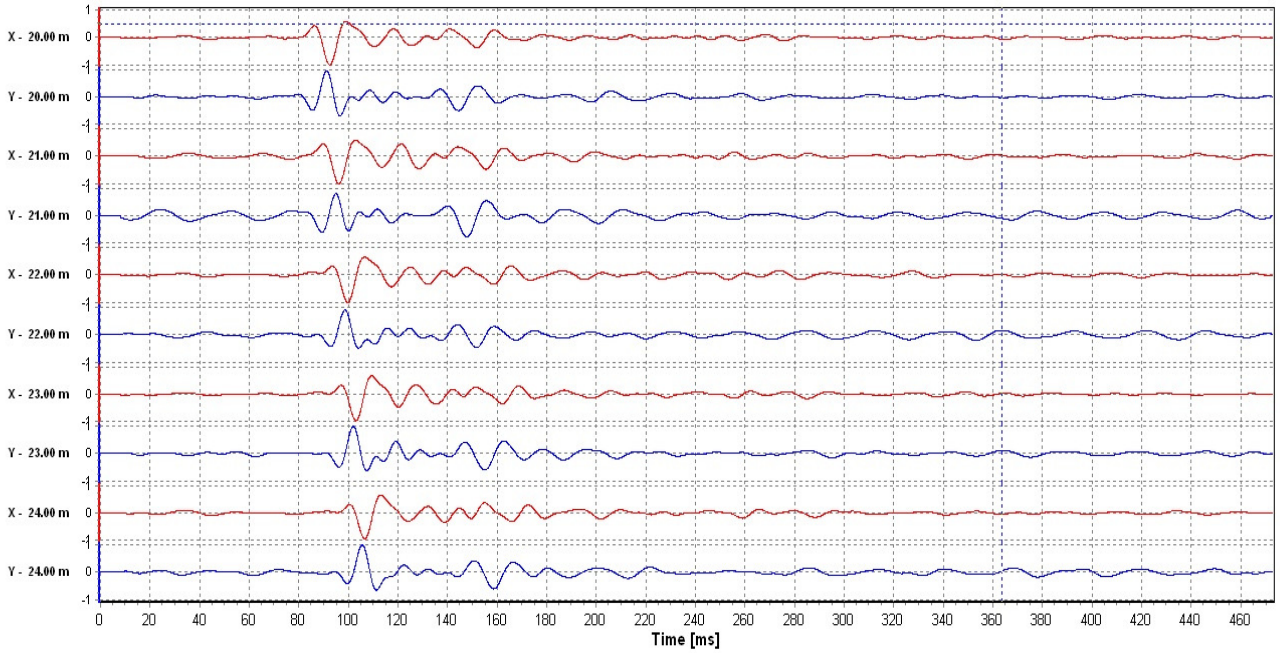

Figure 25: Site SCPT2 LS X(t) and Y(t) axes filtered 20 Hz to 130 Hz where significant "ringing" is present. Option *normalize locally* implemented where it is evident that there are strong responses on both the X and Y axes.

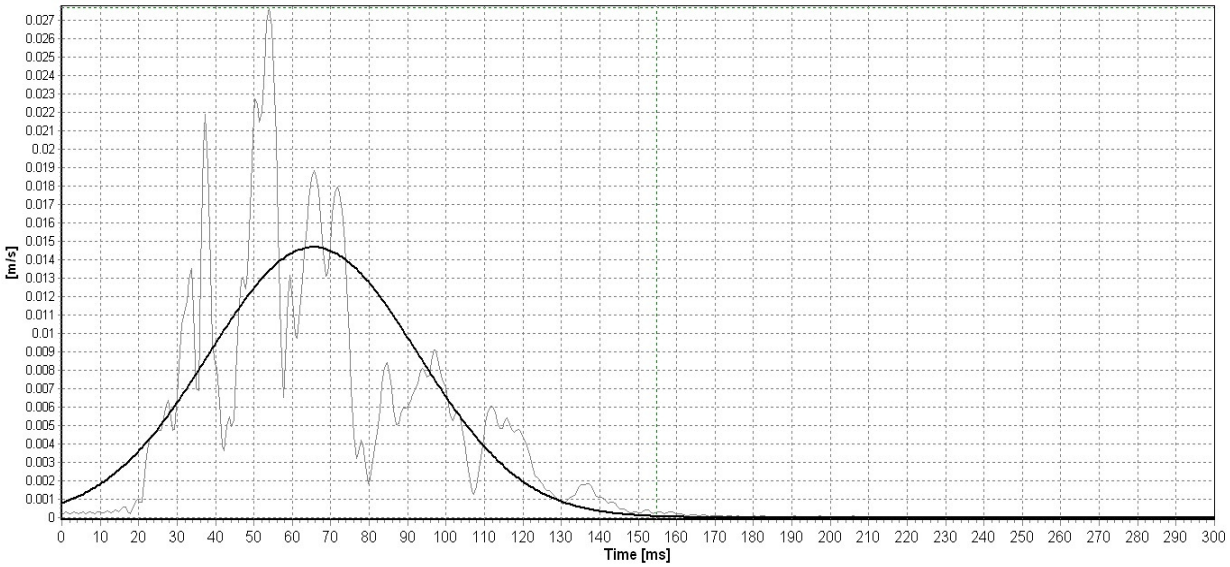

Figure 26: Frequency spectrum (light grey trace) and corresponding "Bell-Shape" best fit (dark black trace) for filtered trace recorded at 22m (X axis dominant response) and illustrated in Fig. 25. The corresponding SSP value is 0.55.

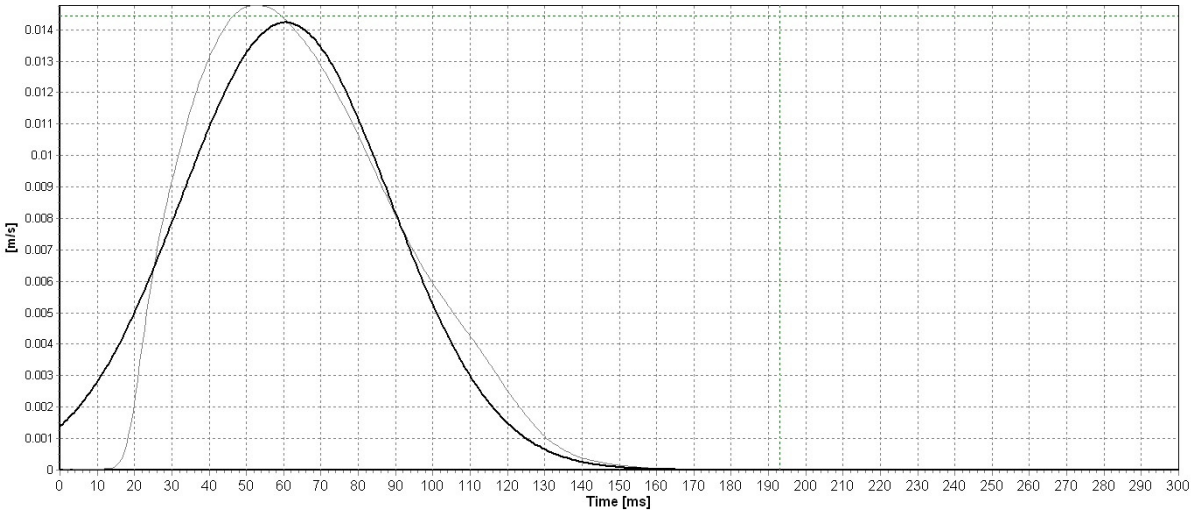

Figure 27: Frequency spectrum (light grey trace) and corresponding "Bell-Shape" best fit (dark black trace) for filtered trace (with time window applied) recorded at 22m (X axis dominant response) and illustrated in Fig. 25. The corresponding SSP value is 0.821.

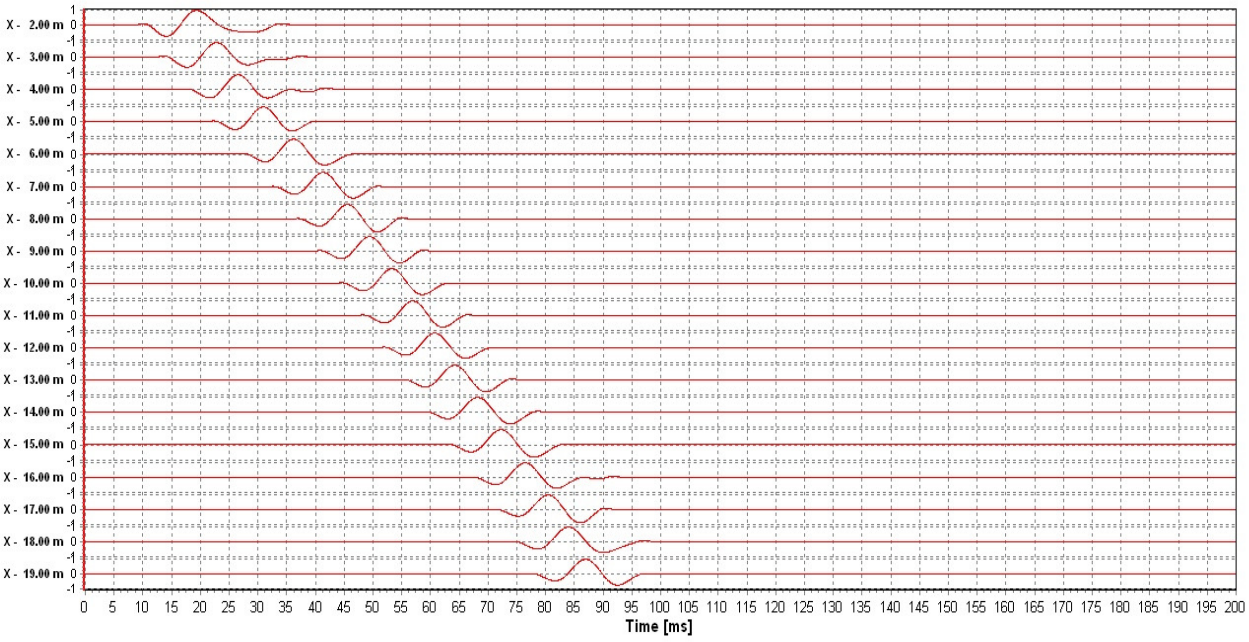

Figure 28: SCPT2 left side full waveform responses.

Table 5. Right Side (RS) and Left Side (LS) Interval Velocity Estimates for SCPT Site SCPT2

Depth [m]	LS Interval Velocity [m/s]	RS Interval Velocity [m/s]	Avg. Interval Velocity [m/s]	Spread
0-2.0	201.2	222.9	212.1	5%
2.0-3.0	235	211.4	223.2	5%
3.0-4.0	229.3	220.9	225.1	2%
4.0-5.0	234.2	209.7	222	6%
5.0-6.0	192.2	199.1	195.7	2%
6.0-7.0	233.1	215.6	224.4	4%
7.0-8.0	282.3	276	279.2	1%
8.0-9.0	242.5	246.9	244.7	1%
9.0-10.0	258.4	259.4	258.9	0%
10.0-11.0	249.8	241.3	245.6	2%
11.0-12.0	244.9	250.4	247.7	1%
12.0-13.0	244	237.6	240.8	1%
13.0-14.0	252.6	252.6	252.6	0%
14.0-15.0	213.8	214.2	214	0%
15.0-16.0	230.7	230.6	230.7	0%
16.0-17.0	241.3	229.7	235.5	2%
17.0-18.0	253.7	255.1	254.4	0%
18.0-19.0	376.6	343.1	359.9	5%
19.0-20.0	304.2	351.2	327.7	7%
20.0-21.0	268.3	267.2	267.8	0%
21.0-22.0	267.4	262.4	264.9	1%
22.0-23.0	326	308.9	317.5	3%
23.0-24.0	279.2	289.8	284.5	2%

The spread is defined as ½ x (LS Interval Velocity – RS Interval Velocity)/Avg. Interval Velocity

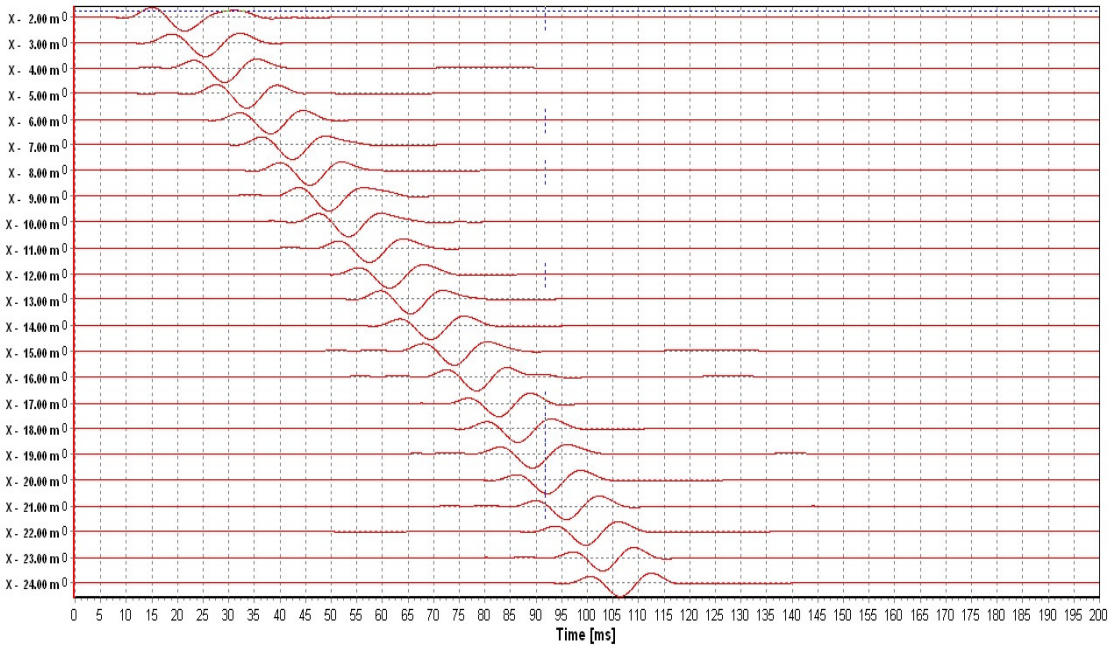

Figure 29: SCPT2 right side full waveform responses.

CONCLUSIONS

Downhole Seismic Testing (DST) is an important geotechnical testing technique for site characterization. DST provides low strain *in-situ* interval compression (*Vp*) and shear (*V*s) wave velocity estimates, but a challenging problem is to obtain a quality assessment of these calculated interval velocities. This paper has outlined a unique interval velocity classification (IVC) technique that uses three seismic time series characteristics. 1) The cross-correlation coefficient calculations of the full waveforms between successive depths of data acquisition. 2) Linearity estimates from the polarization analysis of triaxial or biaxial sensor packages. 3) A new seismic time series characteristic parameter that quantifies the deviation of the source wave frequency spectrum from a desirable bell-shaped curve. The mathematical and implementation details of these three parameters were outlined in this paper. The linearity value obtained from hodograms in PA is a very important parameter within the interval velocity error analysis, due to the fact that linearity identifies signals with low/high SNRs. Hodograms with linearity values nearing 1.0 identify seismic recordings which have highly correlated responses on the X(t), Y(t) and Z(t) axes and strong directionality. This will be the case for seismic traces recorded in TI medium with minimal measurement noise, clean source waves, and no signal distortions (e.g., reflections). The newly developed parameter, denoted as *SSP*, quantifies the deviation of the source wave frequency spectrum from a desirable bell-shaped curve. DST seismic traces with high Signal to Noise Ratios (SNRs) were found to have characteristically bell-shaped curves similar to the probability density of a normal distribution. It was shown when processing real DST data sets that the bell-curve *SSP* value is highly indicative of the SNR of the acquired trace. The application of the IVC was illustrated on two SCPT data sets and with this technique the investigator can assign a confidence indicator for the subsequently estimated interval velocities. In addition, DST seismic traces with low IVC values can be assessed and the investigator can determine to implement more aggressive signal processing algorithms or not use the corresponding low IVC traces for interval velocity estimation. It is the authors' intentions to have this proposed DST interval velocity classification technique evolve, which could involve the incorporation of additional parameters.

REFERENCES

Aki, K. and Richards, P.G. (2002). *Quantitative Seismology (*2nd ed). University Science Books, Sausalito, CA, USA.

Andrus, R.D., Stokoe, K.H., & Chung, R.M. (1999). "Draft Guidelines for Evaluating Liquefaction Resistance using Shear Wave Velocity Measurements and Simplified Procedures." NISTIR 6277. National Institute of Standards and Technology, Gaithersburg, Md.

Andrus, R. D., and Stokoe, K. H., II., (2000). "Liquefaction resistance of soils from shear-wave velocity.'' *J. Geotech. and Geoenvir. Engrg., ASCE*, 126(11), 1015–1025.

ASTM (American Standards and Testing Methods). (2013). "D7400: Standard Test Methods for Downhole Seismic Testing." *ASTM* Vol. 4.09 Soil and Rock (II): D5877-latest.

Baziw, E., and Verbeek, G. (2016), "Frequency spectrum "bell-curve" fitting as a component of SCPT interval velocity accuracy assessment." In Proceedings of the 5th International Conference on Geotechnical Site Characterization (ISC-5), Queensland – Australia, 5-9 Sept. Publisher unknown at this time.

Baziw, E. (2004a). "Two and three dimensional imaging utilizing the seismic cone penetrometer." In Proceedings of the 2nd International Conference on Geotechnical Site Characterization (ISC-2), Porto, Portugal, 19-22 Sept. *Millpress Science Publishers*, 1611-1618.

Baziw, E., and Verbeek, G. (2012). "Deriving Interval Velocities from Downhole Seismic Data." Geotechnical and Geophysical Site Characterization 4 – Mayne (eds), *CRC Press*, 1019–1024.

Baziw, E. (1993). "Digital Filtering Techniques for Interpreting Seismic Cone Data." *Journal of Geotechnical Engineering, ASCE*, Vol. 119, No. 6, pp. 98-1018.

Baziw, E. (2002). "Derivation of Seismic Cone Interval Velocities Utilizing Forward Modeling and the Downhill Simplex Method." *Can. Geotech. J.,* Vol. 39, 1181-1192.

Baziw, E. (2004a). "Two and three dimensional imaging utilizing the seismic cone penetrometer." In Proceedings of the 2nd International Conference on Geotechnical Site Characterization (ISC-2), Porto, Portugal, 19-22 Sept. Millpress Science Publishers, 1611-1618.

Baziw, E., Nedilko, B., and Weir Jones, I. (2004b). "Microseismic Event Detection Kalman Filter: Derivation of the Noise Covariance Matrix and Automated First Break Determination for Accurate Source Location Estimation.", *Pure appl. geophys.* vol. 161, no. 2, 303-329.

Baziw, E. and Ulrych, T.J. (2006). "Principle Phase Decomposition - A New Concept in Blind Seismic Deconvolution." *IEEE Transactions on Geosci. Remote Sensing (TGRS),* vol. 44, no. 8, 2271-2281.

Baziw, E. (2011). "Incorporation of Iterative Forward Modeling into the Principle Phase Decomposition Algorithm for Accurate Source Wave and Reflection Series Estimation." *IEEE Transactions on Geosci. Remote Sensing (TGRS),* vol. 49, no. 2, 650-660.

Baziw, E., and Verbeek, G. (2012). "Deriving Interval Velocities from Downhole Seismic Data." Geotechnical and Geophysical Site Characterization 4 – Mayne (eds), *CRC Press*, 1019–1024.

Baziw, E., and Verbeek, G. (2014). "Signal Processing Challenges when Processing DST and CST Seismic Data containing TIRs." *ASTM International - Geotechnical Testing Journal (GTJ)*, vol. 37, no. 3, 1-21.

Baziw, E. and Verbeek, G. (2014). "Identifying Critical Layers using SCPT and Seismic Source Moveout." In the Proceedings of the 3rd International Symposium on Cone Penetration Testing, CPT'14, May 12-14, 2014 - Las Vegas, Nevada, 357-364..

Campanella, R.G., Robertson, F.T.C., & Gillespie, D. (1986). "Seismic Cone Penetration Test." In Proceedings of INSITU86. *American Society of Civil Engineers (ASCE) Geotechnical Special Publication*. No. 6, 116–130.

Finn, W.D.L. (1984). *Dynamic Response Analysis of Soils in Engineering Practice.* In Mechanics of Engineering Materials. John Wiley & Sons Ltd., New York. Chapter 13.

GE, M. (2003). "Analysis of Source Location Algorithms, Parts 1 and II." *J. of Acoustic Emission*, vol. 21, 14-18 and 29-51.

Ge M., and Mottahed P. (1993). "An Automatic Data Analysis and Source Location System.", Proceedings 3rd International Symposium on Rockbursts and Seismicity in Mines *A A Balkema* Rotterdam, 343-348.

Ge M., and Mottahed P. (1994). "An Automated AE/MS Source Location Technique used by Canadian Mining Industry." Proceedings 12th International Acoustic Emission Symposium Sappora, Japan, Japanese Society for Non-destructive Inspection Tokyo, 417-424.

Gelb, A. (1974). *Applied Optimal Estimation (4th ed.).* MIT Press, Cambridge, Mass, USA.

Gibowicz, S.J. and Kijko, A. (1994). *An Introduction to Mining Seismology.* Academic Press, San Diego, USA.

Ishihara, K. (1982). "Evaluation of Soil Properties for use in Earthquake Response Analysis." International Symposium on Numerical Models in Geomechanics, Zurich, 237-259.

Kanasewich, E.R. 1981. *Time Sequence Analysis in Geophysics (3rd ed.).* The University of Alberta Press, Edmonton, AB. Canada.

Shearer, P.M. (1999). *Introduction to Seismology.* Cambridge University Press, Cambridge, U.K.